Tampere University

Eetu Airaksinen

INERTIAL MEASUREMENT NETWORK DESIGN AND PROTOTYPING FOR INTELLIGENT HYDRAULIC MACHINES

Master of Science Thesis
Faculty of Engineering and Natural Sciences
Examiners: Prof. Jouni Mattila
MSc Pauli Mustalahti
May 2023

ABSTRACT

Eetu Airaksinen: Inertial Measurement Network Design and Prototyping for Intelligent Hydraulic Machines
Master of Science Thesis
Tampere University
Automation Technology
May 2023

Robotisation of heavy machinery requires extensive sensing of the working environment and the motion state of the machine in relation to its environment. Inertial measurements provide a cost effective way of acquiring the pose of the machine and its parts. There are multiple earlier inertial measurement device designs that have been used in the context of heavy machinery automation research. A new, more modular design was proposed and developed as part of this thesis. The new design leverages modern communication features and enables experimenting with different sensors with relatively low effort.

A concept for the new device was first drawn up. After some critical components had been selected, the concept could be turned into an actual design. The design was refined and finalised, after which prototypes could be manufactured. When the functional prototypes proved the design to be working, they could be tested on a hydraulic manipulator, similar to the use case.

The sensor network formed with the new devices proved to perform better than the previously used system. The modularity of the devices enables further hardware development and future improvements. They also provide a platform for developing more sophisticated software with additional features.

Keywords: inertial, measurement, sensor, network, robotising, intelligent, machine

TIIVISTELMÄ

Eetu Airaksinen: Inertiaalimittausverkoston suunnitelu ja protoaminen älykkäitä työkoneita varten.
Diplomityö
Tampereen yliopisto
Automaatiotekniikka
Toukokuu 2023

Raskaiden työkoneiden robotisointi vaatii sekä laajamittaista ympäristön aistimista, että työkoneen oman tai sisäisen liiketilan aistimista ympäristöön nähden. Inertiamittaus on kustannustehokas tapa saada koneen ja sen osien asento mitatuksi. Useita erilaisia työkoneiden automatisoinnin tutkimukseen tarkoitettuja inertiamittauslaitteita on kehitetty aiemmin. Uutta, modulaarisempaa laitetta ehdotettiin ja se kehitettiin osana tätä diplomityötä. Uusi laite hyödyntää moderneja tiedonsiirto-ominaisuuksia ja mahdollistaa erilaisten anturien kokeilemisen suhteellisen vähällä vaivalla.

Uudesta laitteesta luotiin ensin konsepti. Joidenkin kriittisten komponenttivalintojen jälkeen konsepti saatettiin muuttaa varsinaiseksi laitesuunnitelmaksi. Suunnitelman hiomisen ja viimeistelyn jälkeen voitiin valmistaa prototyypit. Kun toiminnalliset prototyypit osoittivat laitesuunnitelman toimivan, voitiin siirtyä niiden koestamiseen hydraulipuomissa, joka vastaa käyttökohdetta.

Uusien laitteiden muodostama anturiverkko osoittautui paremmin toimivaksi, kuin aiemmin käytössä ollut järjestelmä. Laitteiden modulaarisuus mahdollistaa laitteiston jatkokehittämisen sekä parannukset tulevaisuudessa. Ne tarjoavat myös alustan monimutkaisempien, lisätoiminnallisuuksia sisältävien ohjelmistojen kehittämiselle.

Avainsanat: inertia, mittaus, anturi, verkko, robotisointi, älykäs, kone

PREFACE

This master's thesis was done at Tampere University in the Innovative Hydraulics and Automation research group. It was funded by the European STREAM project.

I would like to thank my colleagues for their help and insights. Thanks to my family and friends for their continuous support. Last but not least, thanks to Anni K. for proofreading and emotional support.

Tampere, 8th May 2023

Eetu Airaksinen

CONTENTS

LIST OF SYMBOLS AND ABBREVIATIONS

ADC	Analog-to-Digital Converter
b	bit, the basic digital unit
CAN	Controller Area Network
CAN FD	Controller Area Network Flexible Data-Rate
°	degree, a unit of angle
DOF	Degrees of Freedom
EE	End Effector
EtherCAT	Ethernet for Control Automation Technology
g	gravitational acceleration
GNSS	Global Navigation Satellite System
GPIO	General-purpose Input/Output
h	hour, a unit of time
Hz	hertz, a unit of frequency
I^2C	Inter-Integrated Circuit, a serial communication bus
IHA	Innovative Hydraulics and Automation
IMU	Inertial Measurement Unit
IP	Ingress Protection
LSB	Least Significant Bit
M	mega, a unit prefix denoting a factor of 10^6
m	metre, a unit of length
MCU	Microcontroller Unit
MEMS	Micro-electromechanical Systems
µ	micro, a unit prefix denoting a factor of 10^{-6}
MWM	Moving Working Machine
OTA3M	On-track Autonomous Multi-purpose Mobile Manipulators
PCB	Printed Circuit Board

RIA	Research and Innovation Actions, a type of research funding from the Horizon Europe programme
RTK	Real-time Kinematic positioning
s	second, a unit of time
σ	standard deviation
SoM	Stack on Module
SPI	Serial Peripheral Interface, a serial communication interface
STREAM	Smart Tools for Railway work safEty and performAnce iMprovement, European research project
τ	averaging time
TwinCAT	The Windows Control and Automation Technology, automation suite
USB	Universal Serial Bus
WS1	Work Stream 1, a part of the STREAM project

1. INTRODUCTION

This thesis is part of Work Stream 1 (WS1) of the Smart Tools for Railway work safEty and performAnce iMprovement (STREAM) project under the European Research and Innovation Actions (RIA). The aim of WS1 of STREAM is to enable the use of on-track autonomous multi-purpose mobile manipulators (OTA3M). The use of OTA3M would improve worker safety by reducing human error. It would also reduce railway maintenance costs by shortening the time needed for the operations by up to 20 %, while improving the quality and accuracy of the work. One of the use cases to be demonstrated for the project is to enable automated replacement of railway sleepers from underneath the rails.[1] The proposed solution requires robotisation of road-rail excavators. Roboticised excavators need high-performance motion control, which in turn requires precise measurements of their link angles. Enabling these angle measurements is the focus of this thesis.

1.1 Automated Earth-Moving

Earth-moving can include a multitude of tasks, ranging from pushing and piling earth to excavating precisely around pipes and cables. Moving working machines (MWM) used for these tasks can be equipped with different levels of automation (0 to 5) in regard to both manipulation (M) and driving (D) [2]. The levels range from assisting in manipulation or driving tasks at level (1M, 0D) and level (0M, 1D), respectively, to fully automated operation at level (5M, 5D). As the tasks and automation-levels vary widely in complexity, so does the complexity of the automation systems needed for such tasks. Different kinds of earth-moving MWMs often have manipulators with multiple degrees of freedom (DOF), which affects how much sensing is required for the controlling automation systems.

The varying levels of automation can offload tasks from the operator to said automation systems. They can enable automated condition and fault monitoring, improving overall system efficiency and uptime [3]. Level (1M, 0D) can provide the operator with features such as manipulator-tip control, reducing the need for directly controlling the joints of a hydraulic manipulator, making it easier and faster to operate [4][5][6]. The ultimate automation level of (5M, 5D) for MWMs would enable them to be fully automated, reducing the role of an operator to that of a machine supervisor.

Automating earth-moving in such a way can be very beneficial for many reasons. Com-

puters excel in high precision control, as well as repetitive and monotonous tasks. Humans are more prone to errors due to factors such as fatigue and distractions. Automated MWMs can also operate with higher efficiency by reducing extraneous movements and by adjusting the engine power output to match the power needs of the hydraulic system. Automated control methods enable using additional valves for each hydraulic cylinder to achieve separate meter-in separate meter-out control, further reducing energy consumption [7]. These methods reduce fuel consumption and therefore emissions, as well as wear on the mechanical parts. These machines can also use time more efficiently. Without the need for breaks and by strictly adhering to the prepared plan, an automated machine can get more done during a workday than even an experienced human driver.

When looking to automate earth-moving, the MWM used to perform the tasks needs to be essentially roboticised. This means that the pose of the machine needs to be known precisely. The pose of a machine consists of its position along three axes and its orientation around the same axes in relation to a wider reference frame. Therefore a machine, or any other object in three dimensional space, has a 6 DOF pose. The position along the three axes and the heading angle around the vertical axis for a machine can be acquired by using a global navigation satellite system (GNSS), with a real-time kinematic (RTK) system in a dual-antenna configuration [8]. The angles around the remaining axes can be acquired using an inertial measurement unit (IMU). The pose of a part of a machine is in relation to the frame of the machine itself. Therefore, their poses can be expressed as 3 DOF rotations in relation to the machine and any other parts in-between itself and the machine. In many cases, the parts are restricted to only 1 DOF or 2 DOF motion so that the restricted angle or angles are known and only the unknowns need to be measured. Without the pose of a machine and its parts, accurate control of its movements cannot be reliably achieved. Such closed-loop control is also required for acquiring comparable results when testing hydraulic manipulator systems [9]. Pose estimation for a hydraulic multi-DOF manipulator can be performed either by measuring the extension of the hydraulic cylinders or by measuring the angle of the manipulator joints. In this thesis the focus is on estimating the rotational angles of manipulator links by using IMUs.

IMUs measure acceleration and rotational rate. An IMU includes a three-axis accelerometer and a three-axis gyroscope. Integrating the acceleration measurement results in velocity. When this velocity is integrated, the result is change in position. However, in the context of MWM motion control, most of the measured acceleration is the result of gravitational acceleration. The direction of the measured acceleration can be utilised in estimating the angles of the machine part the IMU is attached to. The rotational rate measurements can be used for more accurately estimating the instantaneous rate of change in the angles.

1.2 Goals and Structure of the Thesis

The goal of this thesis is to design, prototype and test a relatively low-cost inertial measurement sensor network to be used especially in hydraulic excavators but also in other intelligent MWMs. This would enable easy robotisation of such machines for use in automated earth-moving tasks. Ultimately this can be used for automating the railway sleeper replacement, enhancing the efficiency and safety of such operations.

This thesis will be split into three main parts: theory, implementation and testing. First, the theories behind the robotisation of heavy machinery will be explored, including the technologies needed to achieve it as well as the relation of these to the sensor network being worked on. Next, the design and implementation of the sensor network itself will be discussed, by detailing both the hardware and the software that the sensor nodes contain. Finally, the sensor network as a whole will be tested and conclusions made based on the test results.

2. ROBOTISATION OF HEAVY MACHINERY

Robotisation of MWMs usually requires multiple kinds of sensing. For example, to enable high precision control of the motion of the machine, the movement of the machine needs to be sensed. This includes sensing the pose of the machine and its parts. A machine such as an excavator has an actuator with multiple linkages, as Figure 2.1 shows. The pose of the end effector (EE) could be estimated by measuring how much each cylinder is extended, but this usually requires replacing the cylinders with position-sensing cylinders. Therefore it is often more cost-effective to measure the angles of each of the linkages. When the angle and length of each linkage is known, the EE pose can be estimated from the kinematics of the system.

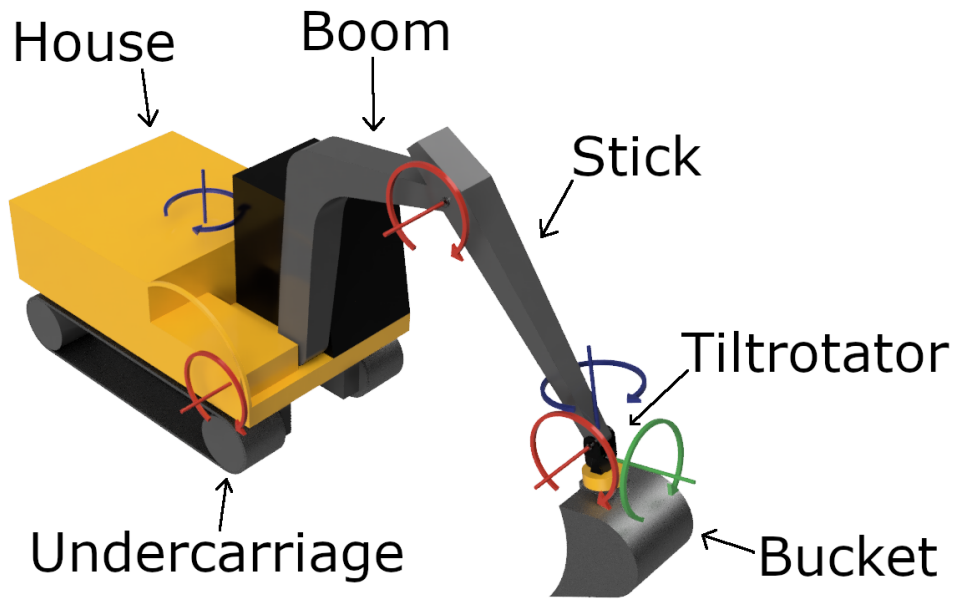

Figure 2.1. *A model of an excavator with an installed tiltrotator with the axes of the joints of the system marked.*

In addition to sensing the machine itself, the machine often needs to sense the world around it. Such sensing can include volumetric information from depth cameras, obstacle detection through LiDAR and computer vision. The data gathered can be used to perform

decisions related to the task at hand or to the safety of any external entities. External sensing can also be used to detect the pose of the machine in a wider reference frame, using technologies such as satellite positioning.

Given adequate programming and enough sensor data about the machine itself and its surroundings, a roboticised MWM can make decisions and act based on those decisions. The decisions can include actions such as how far to move and in which direction, starting and stopping functions related to the task at hand while avoiding collisions with people and obstacles. The decisions can also be about maintenance. As humans are still needed for most maintenance tasks, the system can inform its handlers of any maintenance needs it detects, ranging from refueling to replacing parts.

2.1 Angle Estimation

When implementing motion control in machines, a feedback of the motion is needed to achieve closed loop control. For example, in closed loop control of manipulators, the angles of a moving element are measured and the measurements are compared to the desired angles. This type of feedback requires frequent measurements of the moving elements so that the motion can be controlled efficiently. In a hydraulic manipulator, which is a complex system with multiple joints, the pose of the system reference frame and the angles of the joints can be measured to estimate the pose of the EE using forward kinematics.

In a sense, angle estimation can be compared to proprioception in biological organisms, as it enables an automated machine to sense where its own parts are. This self-sensing is crucial for determining if any parts of the machine are in danger of coming into contact with any obstacles or the machine itself, so that these collisions could be avoided. If the locations of the obstacles and possible avoidable zones are known in relation to the machine and its parts, they can be taken into account when planning the trajectories of the machine parts.

2.1.1 Previous Prototypes

This thesis was done for Innovative Hydraulics and Automation (IHA), a research unit of Tampere University. In previous years, researchers from IHA have used inertial measurement based devices for estimating the motion state of hydraulic manipulators [10][11][12]. The device introduced in [10], developed by previous researchers of the group, is a highly integrated sensor module. It can be sampled at a rate of 500 Hz through a Controller Area Network (CAN) bus and included a Murata SCC1300-D02 IMU sensor and a microcontroller unit (MCU) [10]. The sensor includes a single-axis gyroscope and a three-axis accelerometer. The sensor itself is capable of a sampling rate of 2000 Hz through Serial

Peripheral Interface (SPI), with two separate buses for the gyroscope and the accelerometers [13]. The sensor module is pictured in Figure 2.2.

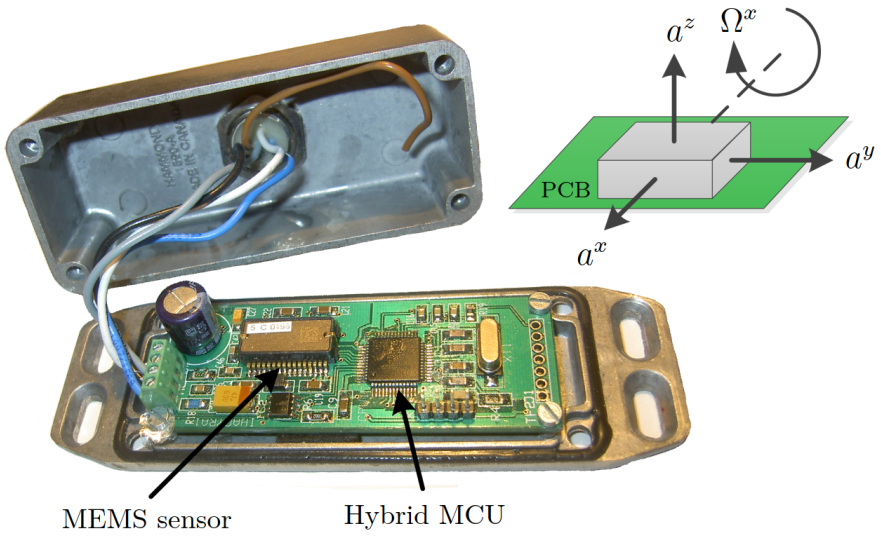

Figure 2.2. *An older sensor module with accelerometer and gyro sensitive axes shown [10].*

Another device, shown in Figure 2.3, was presented in [11]. It features an Analog Devices ADIS16485 iSensor MEMS IMU. The IMU readings are processed by an STM32F407 MCU, which transmits them through CAN bus. The readings are used by the automation system to run a motion control loop at 500 Hz.

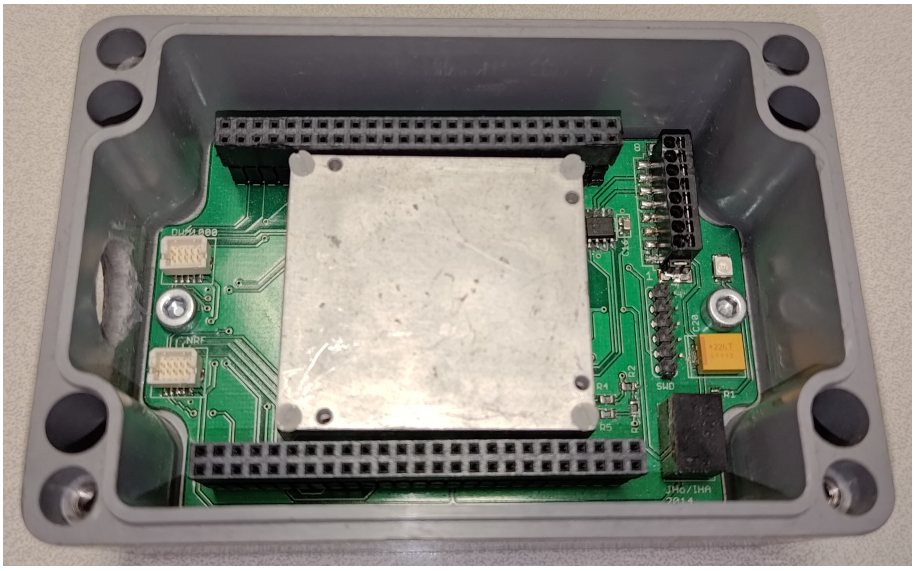

Figure 2.3. *An inertial measurement sensor node with an Analog Devices ADIS16485 IMU.*

The device presented in [12] is shown in Figure 2.4. It has a separate, off-the-shelf STM32 MCU development board connected to a custom base printed circuit board (PCB). The base PCB also has a socket for a commercial IMU evaluation board. The IMU on the evaluation board is a Bosch BM160, which is a low cost, relatively low accuracy sensor. The base PCB in the device includes hardware for interfacing with Ethernet, which is how the measurement data gets communicated off of the device. There is also a modified device with added wireless networking capability.

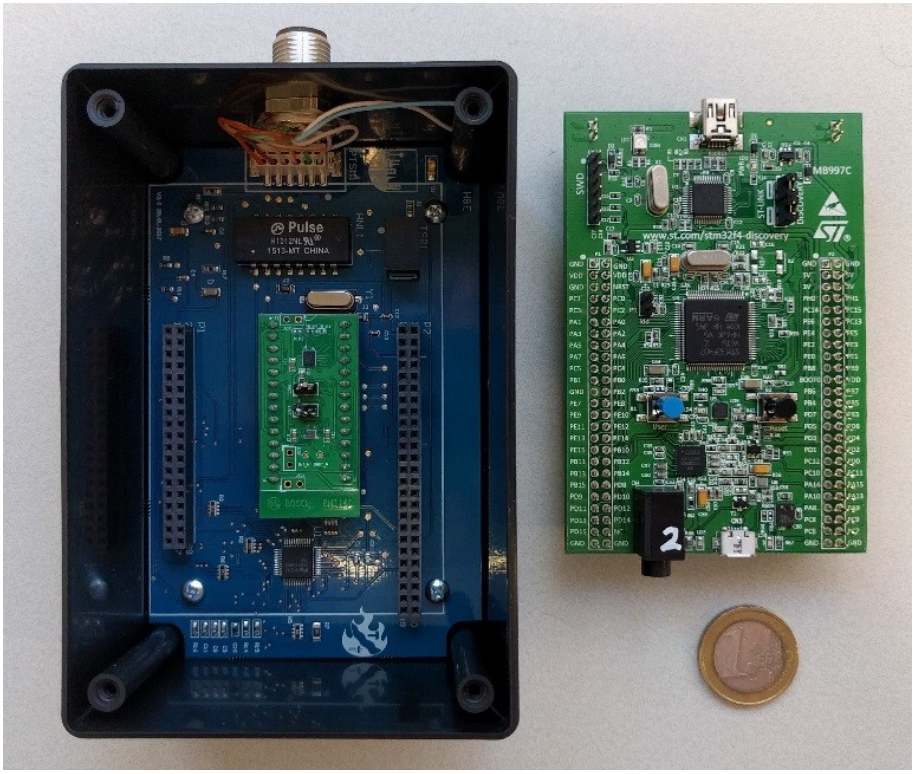

Figure 2.4. *An inertial measurement sensor node with its MCU board removed [12].*

2.1.2 Inertial Measurement

Using inertial measurements of the manipulator movements instead of direct mechanical measurements of joint rotations or cylinder extensions enables easier installation of the sensors without strict mechanical tolerances and high precision mechanical components. As can be seen in Figure 2.5, installing angular measurement sensors to rotational joints often requires the use of flexible couplings to prevent damage to the sensor, as mounting the axles with the required high coaxial tolerances can be difficult. The lack of parts susceptible to wear through friction and mechanical movement in inertial sensors leads to lower maintenance requirements. Inertial sensors can also be easily enclosed in such a way as to make them suitable for the harsh environmental conditions often experienced by MWMs while operating. Environmental protection of electrical and electronic devices is often rated using the ingress protection (IP) rating system [14]. The rating consists of two

numbers, the first of which indicates how well the device is protected against dust ingress. The second number is indicative of the water ingress protection. The meaning of each of these numbers can be seen in Table 2.1. Unlike mechanical joint angle sensors, IMUs do not have axles or other parts needing mechanical pass-throughs that might be vulnerable to water or dust ingress. This makes IMUs easier to protect against the environment by mounting them into simple enclosures with sufficient IP ratings, such as IP65 for a device likely to be exposed to rain. Often a rating of IP67 is required in so-called industrial grade devices to ensure their survivability in a wide range of environmental circumstances.

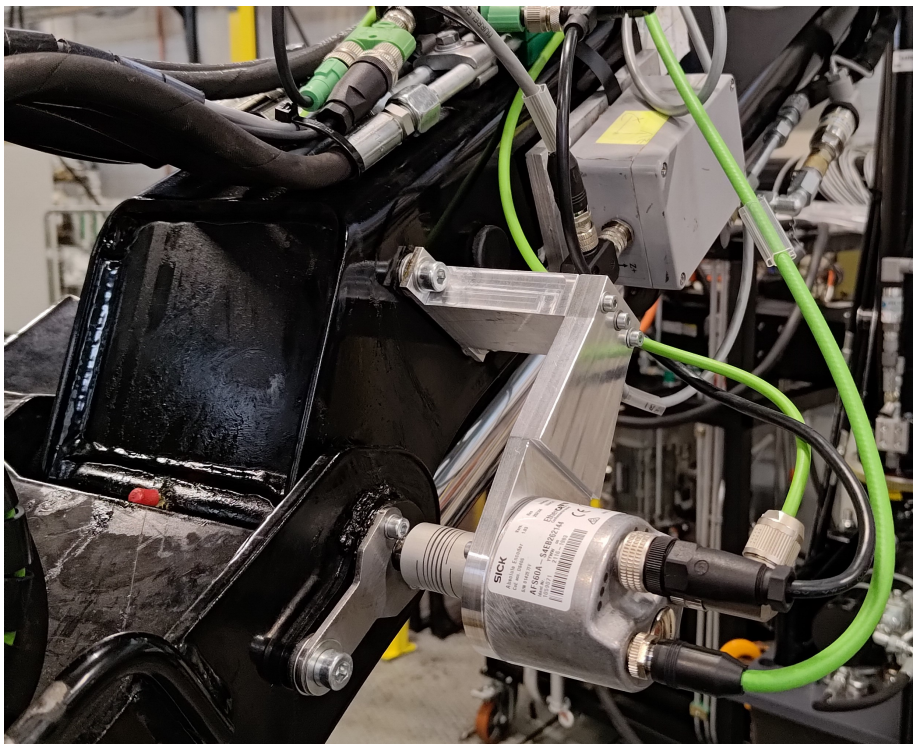

Figure 2.5. *An absolute angle encoder manufactured by SICK, with an older IMU box behind it, mounted on a Hiab hydraulic manipulator used for IHA research purposes.*

Inertial measurement relates to the measurement of acceleration and angular rate of a platform the measuring sensor is attached to. The majority of modern, cost-effective inertial sensors consist of micro-electromechanical systems (MEMS). These are devices with microscopic moving parts, especially in the case of inertial measurement sensors. The movement of these moving parts can be measured through changes in capacitance, for example. The acceleration and angular rate can be inferred from these motions.

Specifically, MEMS accelerometers usually include a mass on a cantilever beam, capable of moving along a single axis. When the system experiences acceleration in the direction of the axis, the mass moves between two fixed electrodes, changing the capacitance between itself and the electrodes. The difference in capacitance between these two capacitors can be measured and used as a measure of the acceleration. Any acceleration measured by a stationary accelerometer is caused by the gravitational acceleration of the

IP**XY**

Dust		Water	
X		**Y**	
0	No protection	0	No protection
1	Protected against solid foreign objects with a diameter of 50 mm and greater	1	Protected against vertically falling water drops
2	Protected against solid foreign objects with a diameter of 12,5 mm and greater	2	Protected against vertically falling water drops when enclosure tilted up to 15°
3	Protected against solid foreign objects with a diameter of 2,5 mm and greater	3	Protected against spraying water
4	Protected against solid foreign objects with a diameter of 1,0 mm and greater	4	Protected against splashing water
5	Dust protected	5	Protected against water jets
6	Dust-tight	6	Protected against powerful water jets
		7	Protected against the effects of temporary immersion in water
		8	Protected against the effects of continuous immersion in water
		9	Protected against high pressure and temperature water jets

Table 2.1. *IP rating test requirements for dust (X) and water (Y) ingress [14].*

Earth. If there is any active acceleration along the measurement axis, this will be added to or subtracted from the gravitational acceleration, depending on the direction. MEMS gyroscopes, on the other hand, generally use two dimensional vibratory systems. A mass is driven to vibrate along the *x* axis and any rotation around the *z* axis causes a vibration to be induced along the *y* axis by the Coriolis force. The amplitude of this vibration can be used as a measure of the angular rate around the *z* axis. [15]

Two examples of contemporary MEMS IMU sensors are shown in Figure 2.6. In an IMU, the accelerometers measure acceleration along three perpendicular axes, whereas the gyroscopes measure angular rate around the axes. This enables acquiring a three dimensional acceleration vector and the rotational rate in three dimensions as well. When the accelerations and the rotational rates are combined, the measurements can be used to estimate the change in the 6 DOF pose of the IMU in relation to a known starting position. In MWMs however, usually only the acceleration measurements are used in estimating a 3 DOF pose, as the starting pose is not known and the rotational rate measurements can only provide information about the rates of change the angles.

The gyroscope data is needed in conventional inertial pose estimation to determine the rotational angles of the platform being measured. In MWMs they are mostly used for continuous rotational rate measurements, as gyroscopes have some limitations that have to be taken into account. MEMS gyroscopes often have drift over time, caused by the rotation of the Earth. This can be observed as a small, constant rotational rate measurement

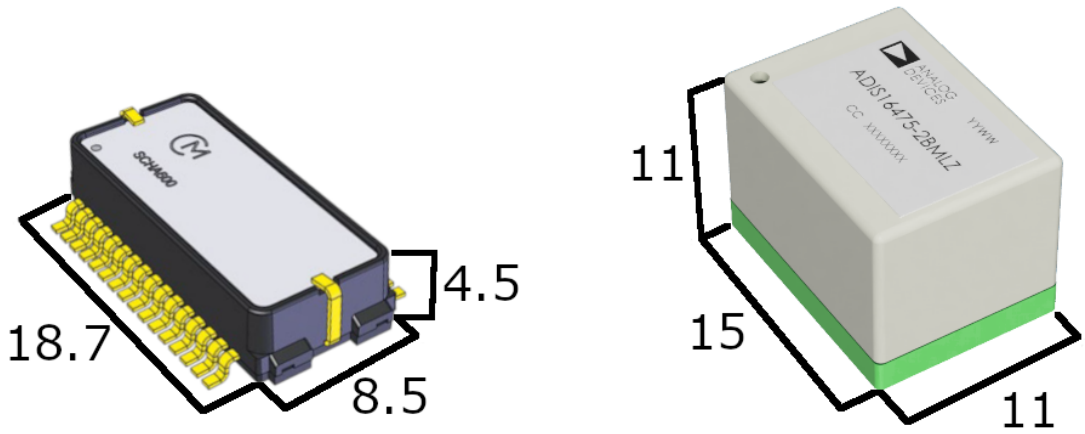

Figure 2.6. *Murata SCHA600 series IMU (left) and Analog Devices ADIS16475 series IMU (right). Dimensions in mm.*

around the vertical axis of the IMU.

Overall, IMUs can be very useful when implementing pose estimation in MWMs, when the raw data is handled in an appropriate manner and combined with data from other sensors. IMUs offer a relatively reliable way of acquiring data about the movements and angles of the parts of the machine, with minor added cost. IMU sensors do not require extensive modifications to machines they are installed on, as they can just be attached with simple straps, magnets, et cetera. This means multiple sensors can be easily installed in various positions to accommodate different kinds of machines.

Modern MEMS IMU sensors incorporate features such as hermetic sealing. Making the sensors airtight in this way improves their survivability in changing environmental conditions and can improve their temperature stability. This can be beneficial, as the readings of MEMS IMU sensors often tend to drift when the sensors are exposed to changes in temperature. Some sensors are factory calibrated to ensure more accurate measurements over a broader range of conditions. Such is the case for Analog Devices ADIS16475 series IMUs, which have dynamic compensation formulas as a result of being individually factory calibrated for sensitivity, bias, alignment, gyroscope bias and accelerometer location [16].

Developments in the technologies used in MEMS IMU sensors have led to increased performance both in the way of the accuracy and the speed of the measurements. For example, the potential resolution of the analog-to-digital converters (ADC) used to acquire the raw readings from the MEMS sensors has increased over the years. It is not uncommon to have IMU sensors with 16- or 20-bit ADCs nowadays, as opposed to the 12-bit ADCs that were common previously. Faster processors embedded into the sensors have led to faster sampling rates and more advanced internal filtering. Table 2.2 lists the

main specifications of three MEMS IMU sensors.

	ADIS16485	SCHA63T-K03	ADIS16475-2
Approx. Year of Introduction	2012	2021	2017
Maximum Sample Rate (Hz)	2460	8400	2000
Gyroscope Range (°/s)	±450	±300	±500
Gyroscope Sensitivity (LSB/°/s)	50	80	40
Gyroscope Bias Stability (°/h)	6.25	1.64	2
Accelerometer Range (*g*)	±5	±6	±8
Accelerometer Sensitivity (LSB/*g*)	4000	4905	4000
Accelerometer Bias Stability (µ*g*)	32	12.2	3.6

Table 2.2. *Comparison between the specifications of Analog Devices ADIS16485 IMU [17], Murata SCHA63T-K03 IMU [18] and Analog Devices ADIS16475-2 IMU [16].*

As Table 2.2 shows, the two newer IMUs are quite similar in their gyroscope bias stability. When compared to the Murata SCC1300-D02 IMU sensor used in the older sensor module, all of these more modern sensors have higher measurement ranges and higher sensitivities [10]. All of the listed IMUs are capable of high sampling rates. These high rates are crucial for achieving smooth motion control, as they are needed for the high-performance signal processing used for joint angle estimations. As the motion controller in a MWM can run at 500 - 1000 Hz, the sampling rates of the sensors should be able to exceed those frequencies.

IMUs can be graded based on their performance factors [19]. One of these factors is their Bias Stability, also known as Bias Instability, In-Run Bias Stability, Bias In-Run Instability or a variation thereof. The sources of this noise are the components, such as electronics, that are susceptible to random low-frequency variations. Table 2.3 lists different performance grades based on Bias Stability. Based on this grading, the IMUs in Table 2.2 would fall in the Tactical grade.

IMU Grade	Accelerometer Bias		Gyroscope Bias	
	m*g*	m s^{-2}	°h^{-1}	rad s^{-1}
Marine	0.01	10^{-4}	0.001	5×10^{-9}
Aviation	0.03-0.1	3×10^{-4}-10^{-3}	0.01	5×10^{-8}
Intermediate	0.1-1	10^{-3}-10^{-2}	0.1	5×10^{-7}
Tactical	1-10	0.01-0.1	1-100	5×10^{-6}-5×10^{-4}
Consumer	>3	>0.03	>100	$>5 \times 10^{-4}$

Table 2.3. *IMU grades based on biases [19].*

Noise performance of gyroscopes can be characterized using the Allan variance method. It enables determining the characteristics of the processes that produce random noise

in the data. By integrating data points in clusters of increasing lengths, Allan variance can be calculated as a function of cluster time. The graph of the function often takes a form similar to the example shown in Figure 2.7. As can be seen, there are multiple other factors, which affect the performance of gyroscopes. Most important ones, in addition to Bias Stability, are Angle Random Walk, Rate Random Walk, Rate Ramp and Quantization Noise. Angle Random Walk is the result of high frequency noise originating mainly from the active elements involved in the measurements within the gyroscope. Rate Random Walk is a process of uncertain origin. Rate Ramp is a deterministic error over long periods of time, possibly originating from slow, monotonic change within the gyroscope or from a slight, persisting acceleration of the platform in a constant direction. Quantization Noise originates from the resolution limitations of the analog-to-digital conversion happening between the MEMS elements and the output of the gyroscope system. Ultimately, Bias Stability is extremely important because it represents the lowest variance of the system, which cannot easily be filtered or calibrated out and results in accumulating error over the operational time of the gyroscope. [20]

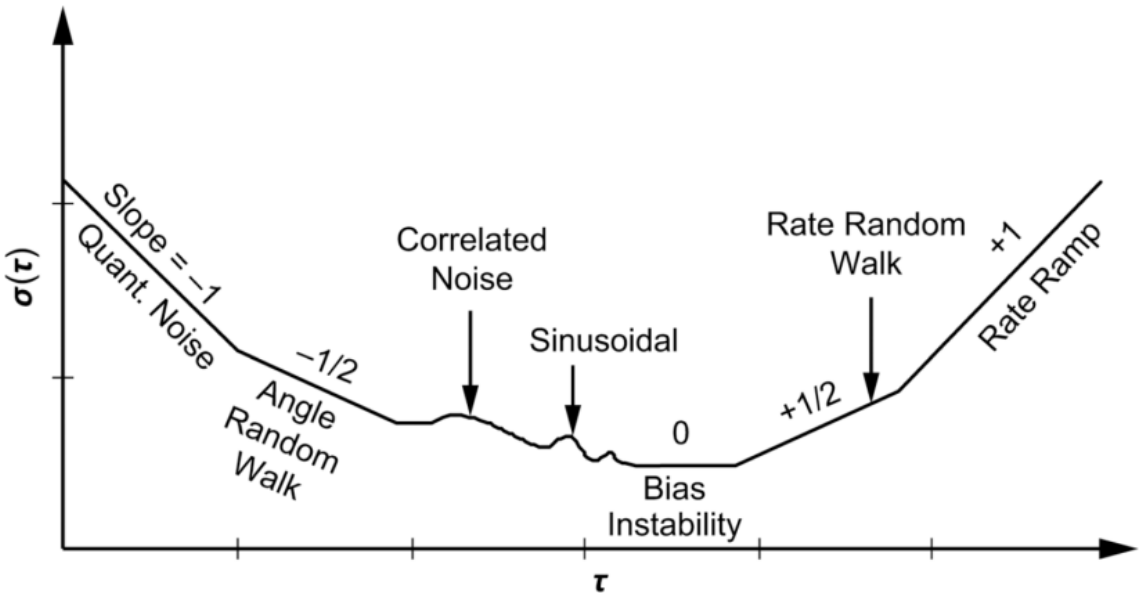

Figure 2.7. *$\sigma(\tau)$ sample plot of Allan variance analysis results [20].*

Allan variance or Allan deviation can be measured for specific sensors to determine their characteristics. An example can be seen in Figure 2.8. It shows the typical Allan variance of the gyroscopes inside the ADIS16475-2 IMU based on the measurements made by the manufacturer of the sensor. Another example is shown in Figure 2.9, as it depicts the average Allan variances of the three gyroscopes within the SCHA63T-K03 IMU. Allan variance is depicted as a log-log plot. In the case of the ADIS16475-2, there are three plots to represent the three gyroscope axes. These plots show very clearly the Quantization Noise and Bias Stability characteristics of the sensor, with Rate Ramp being somewhat varied between the different axes of the gyroscope. The advertised value of 2 °/h for the Bias Stability of the gyroscopes would appear to be correct based on the plots. The Al-

lan variance plot for SCHA63T-K03 would seem to agree with the reported Bias Stability value of 1.64 °/has well.

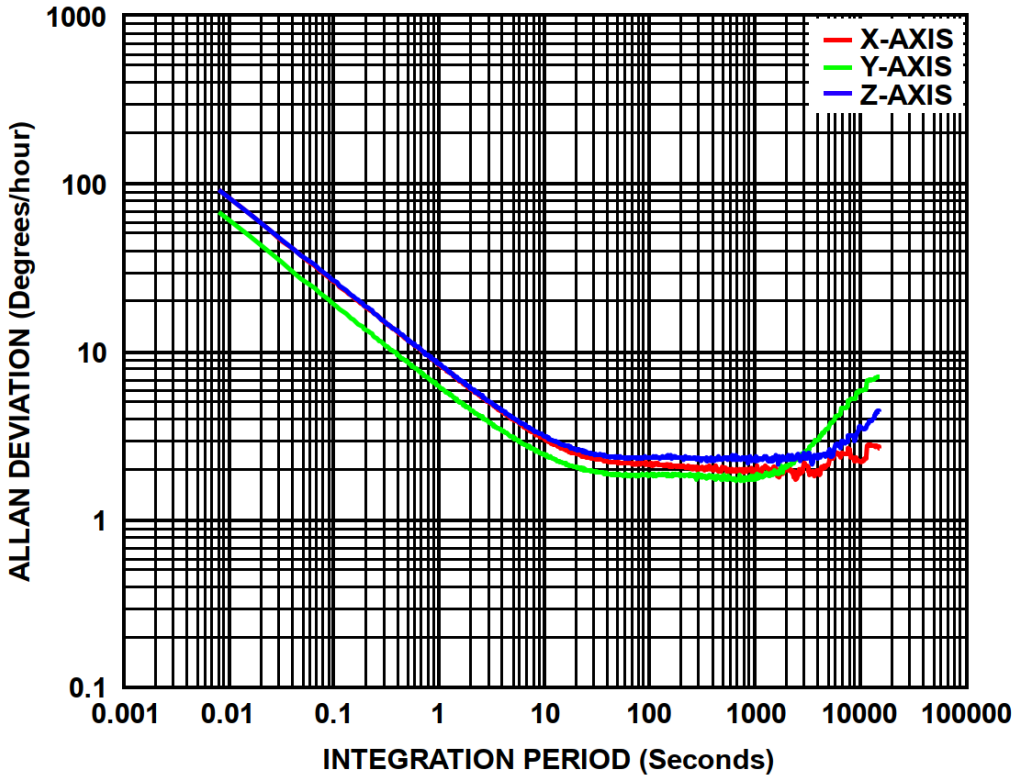

Figure 2.8. *Gyroscope Allan Deviation vs. TC = 25°C, ADIS16475-2 [16].*

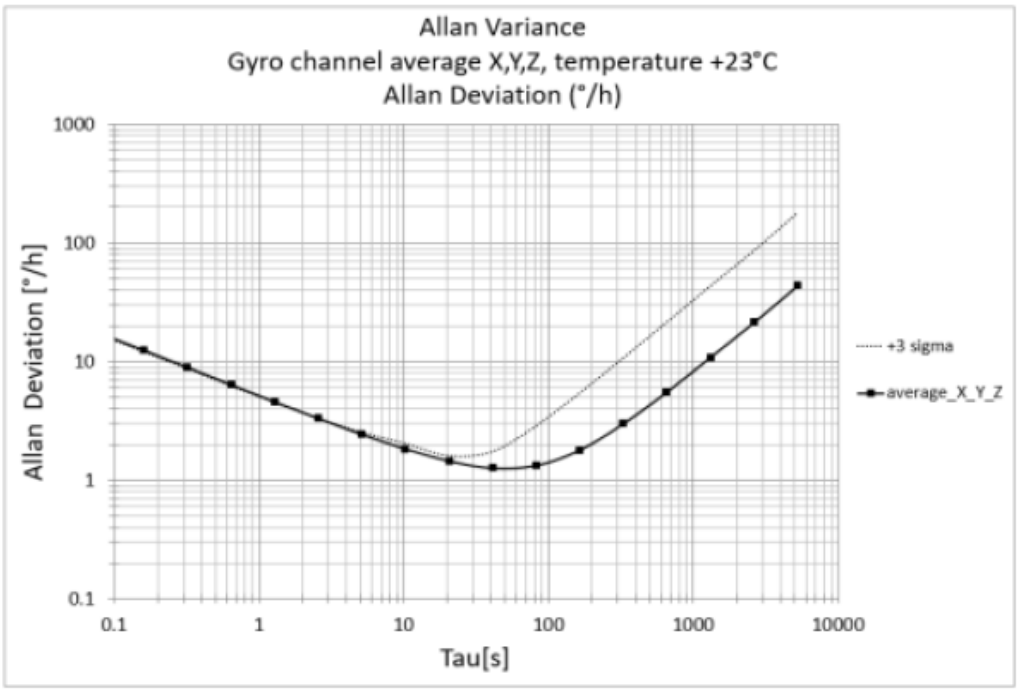

Figure 2.9. *Gyroscope Allan Deviation, SCHA63T-K03 [18].*

2.1.3 Satellite Positioning

IMUs by themselves might not be enough for accurate angle estimation in all use cases. As mentioned above, MEMS gyroscopes have their limitations when it comes to accuracy and drift. Those limitations can be mitigated with other technologies, such as GNSS combined with RTK.

GNSS works by triangulating the location of a receiver on the globe by measuring how long satellite signals have to travel to reach the receiver. This can be extremely useful for determining the position of a device in relation to a wide reference frame. Unfortunately, GNSS is limited to about 3 to 5 meters in its accuracy. Using RTK, this accuracy can be increased by a couple orders of magnitude to about 1 to 2 centimeters. RTK involves having a reference station with a GNSS receiver in a known, fixed location, which can be used to analyze the sky for information about the satellite constellation and the effects of the atmosphere. From this, location correction data can be created, usable by RTK receivers in a 50 kilometer radius from the reference station.

An example of a modern, compact GNSS/RTK chip is the u-blox ZED-F9P, pictured installed on an adapter board in Figure 2.10. In addition to its small size, the chip boasts high update rates and centimeter-level accuracy. These features make it an attractive option for including in miniaturized sensor nodes, enabling accurate motion control. An external antenna is required when using the u-blox chip but the antenna can have a long cable, making it possible to mount it in an optimum location.

2.1.4 Absolute Pose Sensing

With precise location data available, when using two or more RTK receivers, absolute measurements of heading can be made. These absolute but discrete measurements can be combined with continuous inertial measurements for smooth and accurate pose estimation. For example, gyroscopes can be used for instantaneous angular rate measurements, where their drift has no effect. In addition to heading, pitch and roll, RTK can provide the system with very accurate location data, which is important in determining the position of the machine in relation to the reference frame of the work site. The angles in combination with the location coordinates result in a 6 DOF pose.

With the combined data from RTK and IMU, continuous and absolute pose can be acquired. In MWMs, with multiple parts that are moving in relation to each other, absolute pose is only needed for one part of the machine. This can be the house or the undercarriage of an excavator, for example. The pose of the rest of the parts can be inferred from their movement in relation to the absolutely positioned part.

Figure 2.10. *A u-blox ZED-F9P GNSS RTK chip mounted on a custom sensor module board with supporting components.*

2.2 Communication

As the machinery in use is controlled by an automation controller, the sensor data has to be communicated in a standard way. As each sensor provides six different measurements, they cannot be easily transmitted through traditional 4. . . 20 mA current messages. The serial data communications, such as SPI and Inter-Integrated Circuit (I^2C) buses, used by a typical IMU sensor are not robust enough to be used in mobile machines. As both SPI and I^2C buses are mainly intended to be used for communications within devices, they are not especially suitable for use with long transmission lines between devices in electrically noisy environments. Therefore, some type of a fieldbus solution is required. This enables the sensor data to be transferred as packets, while also potentially reducing the need for wiring. A roboticised MWM, such as an excavator, often has multiple moving parts, such as the linkages of an excavator arm. As all of these parts might require at least a single IMU or some other kind of sensor, a bus or network type topology is a more reasonable solution than ordinary point-to-point communication.

For a fieldbus to be implemented, an intermediary device is needed. Such a device should be able to read the sensor data, package it in a way suitable for the automation controller and transmit it through a chosen fieldbus protocol. This must also happen at a relatively

high frequency, preferably at least at 1000 Hz. Based on the previous experiences and the technologies available to the research group, it was decided that CAN bus should be replaced with EtherCAT in future measurement hardware.

2.2.1 CAN bus vs. EtherCAT

As mentioned in subsection 2.1.1, there have been previous instances of IMU systems being developed for use in MWMs by researchers in Tampere University of Technology. In these earlier systems, the network used for communication between the IMU sensors and the controller was a CAN bus. For the new, more modern system being developed, it had been decided that an Ethernet for Control Automation Technology (EtherCAT) network should be used instead. Both of the technologies are widely used fieldbus protocols in the industry, but they have some differences. The CAN bus was introduced in 1986 as a comprehensive serial bus for use in cars, whereas EtherCAT was introduced in 2003 for real-time (RT) requirements of automation technology. As EtherCAT, unlike CAN bus, was designed for hard RT applications, it is much more suitable for the strict speed requirements of motion control systems. In hard RT systems, a missed message deadline is considered a failure, as it can cause damage to the system or external entities. Increased system load must not cause deadlines to be missed either. Mostly, CAN bus can be considered for soft RT applications, where missing messages only degrades the performance of the system. In addition, EtherCAT is deterministic, whereas CAN bus is not. It means that EtherCAT can guarantee a message will be transmitted at a specified time so that the time period is predictable.

Some comparisons between CAN and EtherCAT can be seen in Table 2.4. Data rate is the amount of data in bits a bus is able to transfer each second. Cycle time is the period between the starts of two sequential transfers on a bus. Devices is the amount of devices a bus can handle at a time. Length is the maximum length of cable a bus can handle. For a CAN bus, the desired data rate determines the maximum length of the bus, which, in the case of a CAN bus, is the complete length of the bus from one end to another. EtherCAT devices receive and transmit the data going through them, making them act as repeaters, which means that the maximum cable length for EtherCAT is the length of the cable between devices on the bus, instead of the ends of the bus. A main focus for EtherCAT development was to achieve short cycle times of less than 100 µs, whereas it has not been a consideration for CAN bus; the cycle time of CAN bus can change based on the speed of the bus, the number of devices and the amount of data transferred.

Another major difference between the two bus protocols is the topology of the buses. CAN bus is limited to a linear bus, where the bus is two-ended with termination resistors on both ends and all the connected devices are connected in-between. EtherCAT has more options with three main topologies: Line, Star and Tree [21]. The topologies are

Protocol	Data rate (Mb/s)	Cycle time (µs)	Devices	Length (m)
CAN	1	N/A	127	40
EtherCAT	>100	≤100	65 535	100

Table 2.4. *Comparison of maximum technical characteristics of CAN and EtherCAT buses.*

shown in Figure 2.11. Line is the most similar to the CAN bus, as the bus is ran from the master to the last slave on the bus through the intermediate slaves. Star topology has all of the slaves connected directly to the master, requiring the master node to have at least as many interfaces available as there are slave nodes. Tree topology has multiple junctions that can branch out of the bus. All of these main topologies can be combined to create complicated networks that cater to the specific needs of the application. EtherCAT enables the use of junctions, specialized devices for branching out the bus, which makes implementing different topologies relatively easy.

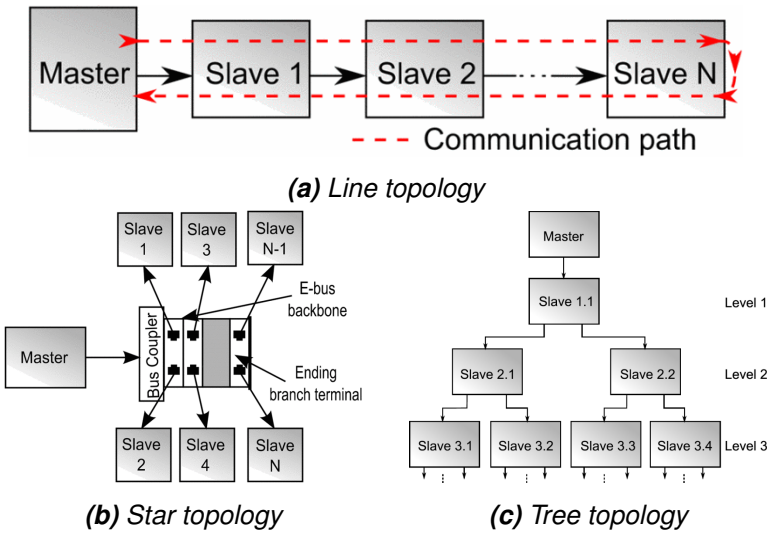

(a) *Line topology*

(b) *Star topology*

(c) *Tree topology*

Figure 2.11. *The three main topologies of EtherCAT-networks [21].*

The topology used in a test setup for the inertial measurement network can be seen in Figure 2.12. In this setup the nodes are installed onto a Hiab XS 033 hydraulic manipulator and connected to the control system through an EtherCAT-network. The line topology was used, as the relatively simple construction of the setup did not require complex branching. The topology could be similar for an excavator arm as well.

As the more modern, feature rich protocol, EtherCAT is more desirable for use in IMU sensor networks in MWMs. Its focus on hard RT communication enables delivering inertial data in a timely manner for use with motion control. Such speeds cannot be guaranteed when using CAN bus, as it is not designed for hard RT applications. There is also CAN FD, which is a faster version of CAN bus (5-8 Mbit/s) with a possibility of using

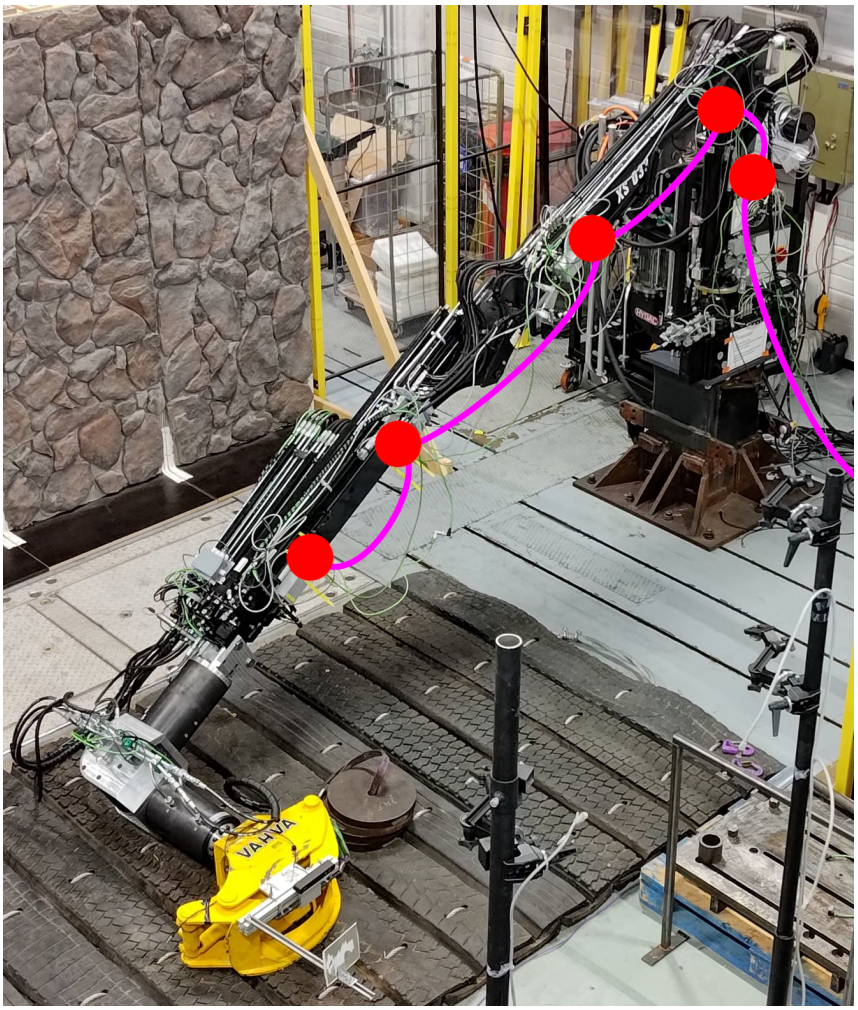

Figure 2.12. *Topology of a test setup. Measurement nodes are shown as red circles and the EtherCAT-network as purple lines. System installed onto a Hiab XS 033 Hydraulic manipulator, used for IHA research.*

longer messages, but it is still much slower than EtherCAT and it does not meet the requirements for hard RT applications either. The ability to create tailored topologies for EtherCAT-networks is a plus when using the bus on machinery with moving parts.

2.3 Complete Inertial Measurement Solution

For use in MWMs, a complete IMU node system has certain requirements. Some of the requirements relate to the expected operating environments of the sensors. Performance figures are a crucial aspect as well. As mentioned earlier, communication capabilities need to be considered too. To figure out some guidelines for the requirements, datasheets of some commercial products were examined.

2.3.1 Commercial Options

There are many commercial products with the same or similar intended use cases as the sensor nodes developed as part of this thesis. These are often meant for pose sensing in vehicles. They include both IMUs and GNSS/RTK receivers. Some examples with their most important specifications are listed in Table 2.5. The table shows some similarities and some differences between the commercial solutions.

	OxTS AV200	Parker 3DMGQ7	Kindhelm IPESSA Nano	SBG Ekinox-D
Position Accuracy (m)	0.05	0.02	0.01	0.01
Velocity Accuracy (m/s)	0.56	0.05	0.05	
Roll/Pitch Accuracy (°)	0.1	0.1	0.05	0.02
Heading Accuracy (°)	0.2	0.25	0.1	0.05
Gyro Bias Stability (°/h)	5	1.5	1.5	<0.5
Data Rate (Hz)	100	1000	100	200
IP Rating	-	-	IP68	IP68
Interface	CAN, Ethernet	Serial, USB	CAN, Serial	CAN, Ethernet, Serial

Table 2.5. *Comparison between four commercial IMU senors.*

The OxTS AV200 [22] seems to be the least accurate overall, only beating the Parker 3DMGQ7 [23] narrowly in heading accuracy. The Parker model itself appears to be the second least accurate, but provides the highest data rate by far, being 5 to 10 times faster than the others. The Kindhelm IPESSA Nano [24] looks to be the second most accurate, while being hampered by its slow data rate, which it shares with the OxTS model. Overall, the SBG Ekinox-D [25] would seem to be the most accurate of all of the sensors, but even it has a relatively low update rate. All of the devices use MEMS IMUs.

Only the Kindhelm IPESSA Nano and the SBG Ekinox-D use industrial connectors which allow them to have an IP rating. The rating often required by industrial applications is IP67 or IP68. Therefore the water resistance of these devices is very good, even allowing immersion in water for limited times. Usually MWMs are not subjected to quite such conditions, though.

While all of the sensors have at least passable accuracy figures, they all suffer from one crucial flaw: insufficient interfaces. The Parker 3DMGQ7 might achieve its barely acceptable data rate by utilizing its Universal Serial Bus (USB) interface. USB interfaces are not usually very suitable for networked architectures or industrial applications. It also is not usable in hard RT applications. Similarly, serial interfaces cannot be networked and

are often relatively slow. Most of the sensors support CAN bus communication, which is too slow for the intended application, as noted previously. Couple of the sensors support Ethernet, which is closer in bandwidth to the desired EtherCAT bus, but still does not have the same robustness or focus on hard RT.

2.3.2 Final Prototype Requirements

For designing the actual system to be used, some guidelines were needed for selection of components and parts of the system. Based on the projected needs of the hardware and by observing the specifications of some similar commercial options, an attempt was made to find out realistic minimum requirements for the measurement nodes. Table 2.6 shows these approximate minimum requirements.

IP Rating	≥ 65
Gyroscope Bias Stability (°/h)	≤ 2
Accelerometer Bias Stability (µ*g*)	≤ 15
ADC Resolution (bits)	≥ 16
Sample Rate (Hz)	≥ 1000
Interface	EtherCAT

Table 2.6. *Minimum requirements for the specifications of the inertial measurement sensor node hardware.*

As the prototype system was not planned to be installed on machines operating underwater, IP65 would be sufficient for environmental protection in research purposes. This should provide protection from rainwater and other effects of weather. As previously mentioned, IP67 or IP68 is usually the required rating for industrial or commercial products. If better IP ratings are needed, the measurement nodes can be housed in better enclosures or the enclosures can have silicone or epoxy cast into them. Casting can also improve the reliability of connectors within a device but it would also make it more difficult or even impossible to repair it. Alternatively, a conformal coating could be used on the surface of the circuit boards and components to shield them from any water entering the enclosure. The values for gyroscope bias stability and accelerometer bias stability were deemed adequate based on the performance of available, cost-effective IMU sensors as well as the performance of commercial solutions.

EtherCAT was the communication interface of choice because it would provide high enough performance and enable easy integration into test systems. The prototypes should be able to provide a sample rate of 1000 Hz or more. The high sample rate makes it possible to implement smooth and accurate motion control in MWMs. The hard RT capabilities of EtherCAT means it has low and predictable latency, which is the delay between an event and a response. Its synchronised signals reduce jitter, which is the variation in latency.

Low jitter is essential in multi-link motion state estimation.

The system was to be a flexible platform for use in research purposes. It would enable testing new IMU designs and a wide variety of other sensors and devices. The system can act as a distributed RT sensor network for use in motion estimation and control as well as other research tasks. It should be able to be programmed using Mathworks Simulink, enabling rapid firmware modifications [26].

3. DESIGN OF HARD REAL TIME SENSOR NETWORK MODULES

A sensor network was built for communicating all of the data from all of the sensors to the automation controller. Using EtherCAT, the network can be built with a topology that suits the geometry and the needs of any specific machinery. EtherCAT also enables RT data transfers. With almost instant data available from multiple sensors, accurate motion control enabling pose estimation becomes possible.

The measurement network consists of nodes with IMU and/or GNSS/RTK sensors installed. For these nodes, a new design was proposed. The aim of the new design was to increase the modularity of the nodes in comparison to previously used designs, while decreasing complexity and, potentially, cost of the nodes. The increased modularity enables more flexible new sensor module prototyping according to different use cases. The same node hardware could be used with new sensors that may be released in the future as well as many different types of sensors for measuring other kinds of physical quantities. Implementing other sensors only requires the design and manufacture of simple, small adapter boards in addition to reprogramming the microcontroller unit (MCU) in the node to read the new sensor via SPI or I^2C.

For the actual design of the printed circuit board (PCB) to be used in the nodes, an electronic design automation software called Autodesk Eagle [27] was used. The software in question is a powerful electronics design tool, while being relatively simple to use. The project files it produces can be later edited if new hardware revisions or additional adapter boards are needed. Autodesk provides an education license for the software, which can be used in an education setting for non-profit purposes.

3.1 Designing Pose Measurement Sensor Node Hardware

A concept for the measurement node hardware was created. A block diagram drawing depicting said concept can be seen in Figure 3.1. The node includes an MCU, headers for attaching sensor modules, a module for EtherCAT communication and some supporting hardware. Figure 3.2 shows what the actual PCB design ended up looking like.

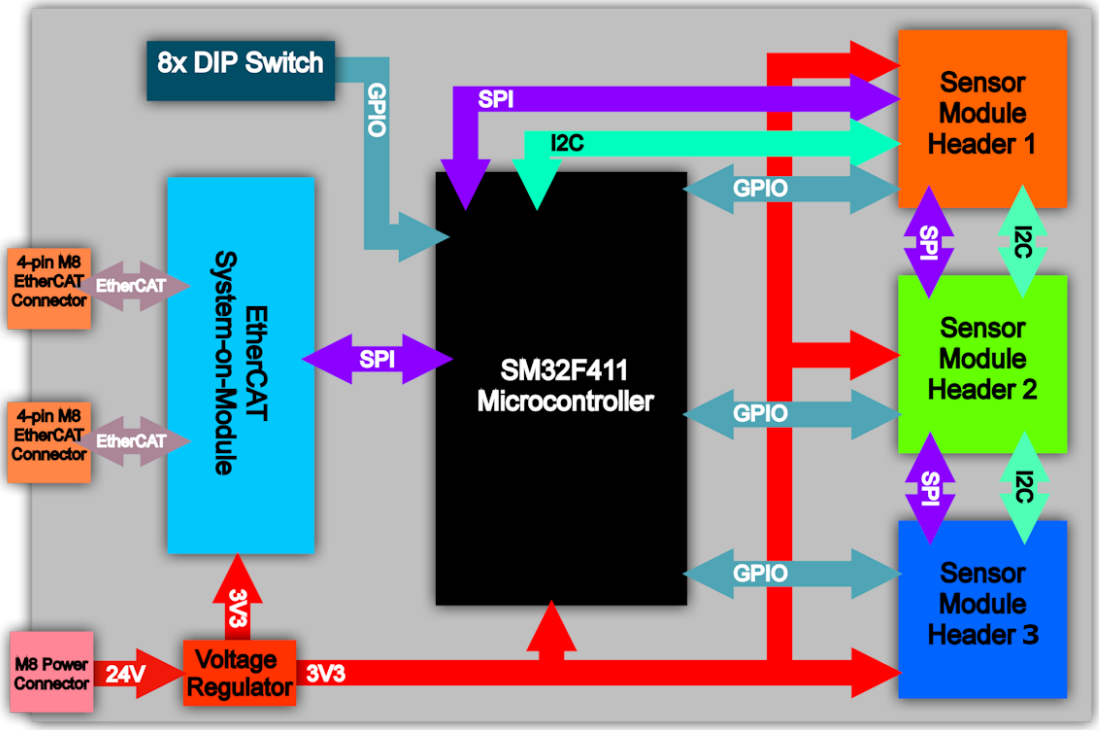

Figure 3.1. *An initial block diagram drawing of the measurement node hardware.*

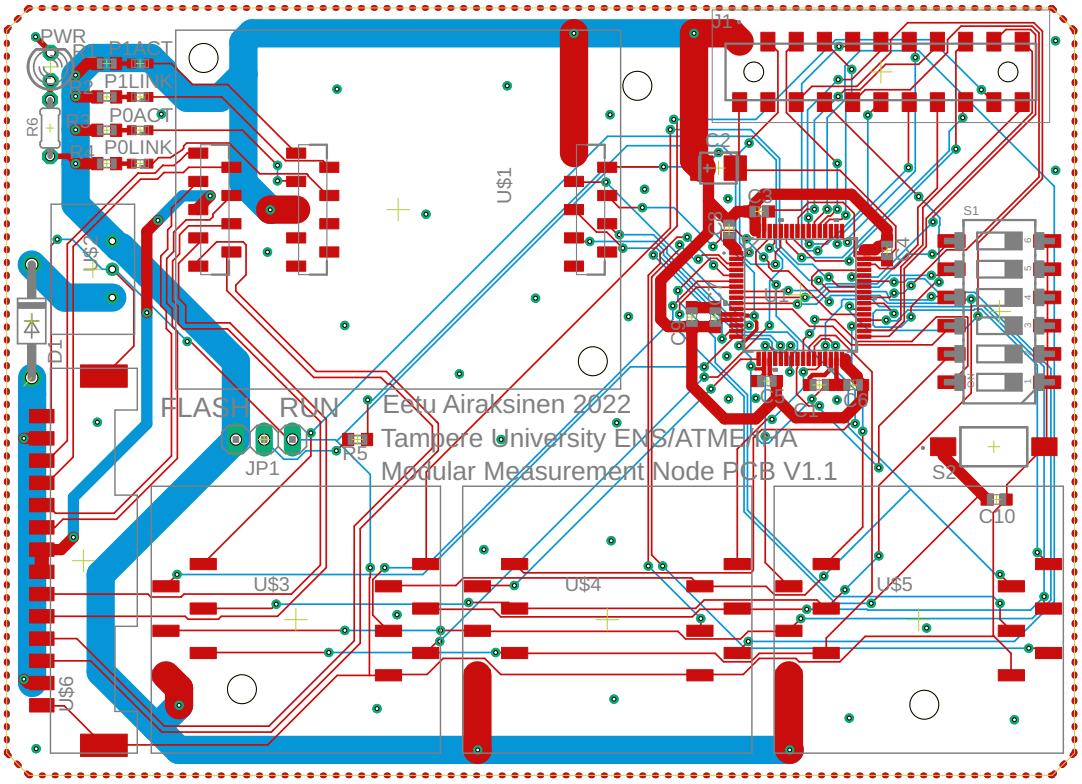

Figure 3.2. *The finished PCB design.*

The supporting hardware on the board includes a voltage regulator, some switches for possible configuration of the firmware, connectors for interfacing and all the passive components required. The completed PCB with all of its components is visible in Figure A.2.

The hardware was enclosed in a cast aluminium case with IP65 rating. In the environments the measurement nodes are expected to operate, prevention of water and dust ingress is very important. Resilience to mechanical stress and impact damage is also beneficial for the lifespan of the hardware. In addition, a sturdy case provides a stable platform for mounting the IMUs.

3.1.1 Microcontroller

The MCU to be used in the measurement nodes was decided based on the available features and compatibility. Early on, it was decided that the hardware should be programmable using Mathworks Simulink [26], as it was seen as an easier way of making changes to the firmware. This decision made it quite easy to determine the MCU to be used. Even though Simulink supports a few different types of MCUs, the STM32 line by STMicroelectronics was an obvious choice based on their availability and the processing power they offer. There is a Simulink Coder support package for STMicroelectronics Nucleo boards [28] which seemed to be a good option for the task at hand. Based on the hardware supported by the package, it was decided that the STM32F411RE MCU [29] would be used. The MCU had enough features, such as communication peripherals, and adequate processing speed for use in the measurement nodes. The chip was also quite affordable, which made it viable to be used in a network which would include multiple measurement nodes. The selected MCU has a clock speed of 100 MHz, which can be achieved using its internal oscillator, minimizing the need for external components. With an external crystal absent, only some capacitors are needed for voltage stabilization. With its full clock speed, the MCU has the capability to communicate on three SPI buses at speeds of up to 50 Mb/s, with two buses limited to a speed of 25 Mb/s. In the sensor nodes, most of the communication being done by the MCU happens through SPI, with one bus dedicated to the sensors and another one to the EtherCAT communication system. As such, by using the faster buses, the MCU should theoretically be able to transfer data at the full 50 Mb/s speed between the two destinations. Some sensors might require communication through an I^2C bus. For such cases the sensor module headers include pins for I^2C as well as SPI. The MCU also has many general-purpose input/output (GPIO) pins, which are very useful in many cases. For example, they can be used as inputs to read the state of configuration switches or as outputs to reset connected sensors.

When the design of the sensor node hardware was being finalized, global supply chain issues were affecting the availability of all kinds of MCUs. In the case of the STM32F411RE, the lead times reported by many suppliers delivering to Finland were at least multiple

months long. This lead to the following option to be considered: purchasing STM32 Nucleo development boards with the appropriate MCU on them, desoldering the chips and soldering them onto the custom sensor node PCBs. The development boards cost approximately twice as much as the bare chips, but at least some were available to order. Fortunately the PCB fabrication company that ended up manufacturing the boards happened to have the correct MCU in stock and could deliver the PCBs with most of the components installed.

3.1.2 Exchangeable Sensor Modules

There was a need for flexibility in the use of the sensors in the measurement nodes. This led to a design that includes multiple positions for exchangeable sensor modules. On the final PCB, there are three available positions. These enable the use of different types of sensors in the same node, or even the use of redundant sensors for more critical applications. The module connectors include SPI and I^2C buses for communication, as well as some GPIO.

Most of the nodes in the network would usually have an IMU installed in them. In some cases, however, the IMUs by themselves might not be enough. In these situations, GNSS/RTK receivers could be used. The three sensor module positions on the circuit board can enable for example the use of a GNSS receiver simultaneously with a discrete gyroscope and a discrete accelerometer.

For the initial test and use of the system, a selection for a sensor was made. It was decided that an Analog Devices ADIS16475-2 [16] IMU would be used. The sensor is not very affordable but it is easy to use and it has very good accuracy. It should therefore showcase the features of the system.

3.1.3 EtherCAT Stack on Module

For communication with the automation system through EtherCAT, a Stack on Module (SoM) by port GmbH [30] was chosen. The iRJ45 is essentially a daughterboard that connects on top of the node PCB. It includes all of the hardware, such as the signal transformers, needed for using EtherCAT communications. There is also a Renesas MCU running proprietary firmware on the module. The host STMicroelectronics MCU interfaces with the EtherCAT SoM using an SPI bus.

However, to get the EtherCAT SoM to work, simply sending data through SPI is not enough. The EtherCAT SoM has its own set of drivers that need to be run on the host STM32 MCU. These drivers initialize the module and provide the data to it in a form it understands. The module also needs some configuration data to be present on its on-board memory in order to operate correctly as an EtherCAT slave device.

There exists a variation of EtherCAT called EtherCAT P, which stands for 'EtherCAT + Power'[31]. With additional circuitry, it should be possible to power the sensor nodes through the signal cables, reducing cabling. If a need for such a modification arises, the extra circuitry can be implemented on a small daughterboard or the design of the node PCB can be modified to incorporate the needed components.

3.2 Sensor Node Firmware

As mentioned, the firmware for the measurement nodes started being developed using Mathworks Simulink. This would have enabled the firmware to be easily reconfigured without the need for particular programming skills, if needed. Software made using Simulink is in the form of models, consisting of interconnected functional blocks. The pre-existing selection of blocks available in Simulink is quite varied, with the Simulink Coder support package for STM32 processors adding some blocks specific to such MCUs.

In the end, porting the EtherCAT SoM drivers to Simulink proved too challenging in the scope of this work. Hence, a decision was made to write the node firmware in the C programming language. Using the dedicated development environment provided by STMicroelectronics and the code examples provided by port GmbH, it was possible to get the MCU to communicate with the EtherCAT module as intended.

The firmware of a measurement node does the following: read configuration switch positions to determine the installed sensors; initialize the sensors; initialize the EtherCAT module; read and package sensor data; write the data out to the EtherCAT module. Notably, at the moment, no filtering of the measurement data is done on the MCU. This means there is no need to do actual calculations on the sensor data on the nodes themselves, as the data will be passed on to much more powerful hardware through the EtherCAT connection, reducing performance overhead on the nodes. This enables fast, continuous streaming of the sensor data, which is important for efficient control of the movement of the machinery the sensor network is installed on. It should be possible to use the processing power of the nodes to do some kind of processing of the sensor data.

The firmware was able to read an Analog Devices ADIS16475 IMU through an SPI bus at up to 2000 Hz frequency by utilising the Burst Read Function implemented on the sensor. This had the downside of only acquiring acceleration data at 16 bit resolution instead of the maximum of 20 bits. 16 bits of resolution is adequate for controlling heavy machinery, however, and the more important measurements of angular rates were received at the full 16 bit resolution of the ADCs in the gyroscopes. If acceleration data is needed to be read at the full 20 bit resolution, the firmware can be modified to do so.

As the rate of 2000 measurements per second was slightly excessive, the Decimation Filter of the ADIS16475 was utilized so that the rate could be lowered to a more reasonable

value. This was enabled by setting a register called DEC_RATE to 1. As the nominal output rate of the sensor is equal to $2000/(\text{DEC\_RATE}+1)$, this resulted in an output sample rate of 1000 samples per second [16]. A frequency of 1000 Hz is still fast enough for achieving smooth motion control, but does not stress the measurement handling hardware extraneously.

With the Decimation Filter set and the sensor enabled, the sensor would pulse its Data Ready signal at the desired frequency of 1000 Hz, to indicate that new measurement data was ready to be read. This signal was connected to an external interrupt pin of the MCU. Whenever the MCU detected a rising edge, it executed a function, which would use the SPI bus to write out two bytes (0x6800), followed by 20 bytes of zeros to the sensor, while reading back the data from it. The data included the diagnostic status of the sensor, the gyroscope measurements of all axes, the accelerometer measurements of all axes, the internal temperature of the sensor, a data counter and a checksum value. Starting from 0, the data counter would increment by 1 every time new data was loaded to the output registers of the sensor and would wraps around back to 0 after reaching 65535.

After the inertial measurements had been read from the sensor, a checksum calculation was performed to verify the integrity of the data. The following formula [16] was used, treating each byte in the formula as an unsigned, 8-bit number:

```
Checksum =  DIAG_STAT, Bits[15:8] + DIAG_STAT, Bits[7:0] +
            X_GYRO_OUT, Bits[15:8] + X_GYRO_OUT, Bits[7:0] +
            Y_GYRO_OUT, Bits[15:8] + Y_GYRO_OUT, Bits[7:0] +
            Z_GYRO_OUT, Bits[15:8] + Z_GYRO_OUT, Bits[7:0] +
            X_ACCL_OUT, Bits[15:8] + X_ACCL_OUT, Bits[7:0] +
            Y_ACCL_OUT, Bits[15:8] + Y_ACCL_OUT, Bits[7:0] +
            Z_ACCL_OUT, Bits[15:8] + Z_ACCL_OUT, Bits[7:0] +
            TEMP_OUT, Bits[15:8] + TEMP_OUT, Bits[7:0] +
            DATA_CNTR, Bits[15:8] + DATA_CNTR, Bits[7:0]
```

The resulting value was compared to the checksum value acquired from the sensor with the burst read. If the values matched, the data could be considered valid. If the data was invalid, it would simply be discarded to avoid any errors in the measurements sent to the automation controller. During testing, no corrupted data packets were detected.

Valid data would be saved to variables, which would be read by the EtherCAT driver code. The code would write it out as Process Data Objects (PDO) into the EtherCAT frame, utilising CANopen over EtherCAT (CoE). A new frame would be sent every time a query was received from the EtherCAT master.

3.3 Communication Layer

EtherCAT provided a fast network for communicating the data between the measurement nodes and the automation controller controlling the system. With it, different topologies could be used if needed. Adding EtherCAT slaves, such as new nodes, other sensors or actuators to the EtherCAT network would be relatively trivial. Separate networks could also be used for the purposes of redundancy or testing. The automation controller would act as the EtherCAT master and with additional network interface cards, could have multiple networks connected to it.

3.3.1 Connection with the Automation System

The systems used for testing and prototyping had automation systems based on Beckhoff industrial computers. The computers run an automation suite called The Windows Control and Automation Technology (TwinCAT). It enables RT computing, making it possible to run efficient control loops on flexible systems.

The TwinCAT system runs software which reads the PDOs from the measurement nodes. The PDOs contain the measurement data from the IMUs. Each measurement, three for angular rate and three for acceleration, is contained in its own PDO. After reading the data into the appropriate variables, the TwinCAT system can record, modify and act based on the data. It would be possible to transmit other data through PDOs as well, if there was a need for it in the future.

3.4 Implementation of the Hardware

After completing the design of the sensor nodes, it was time to implement them. This included manufacturing of the electronics and assembling them into enclosures. Finally, the firmware was also flashed onto the MCUs to make them functional.

3.4.1 Printed Circuit Boards

The PCB manufacturing was subcontracted to a company specialising in electronics assembly. The company had most of the required components in stock, which enabled them to assemble the PCBs automatically using pick-and-place machines. This reduced the need for manual assembly greatly. Only a few specialized connectors and a voltage regulator for each PCB had to be sourced and installed manually. The final assembly operations were completed in an electronics workshop at the Hervanta campus of the University of Tampere.

Figure 3.3 shows a completed sensor node with all of its PCBs. The base PCB has

the MCU, supporting components and connectors on it. The small PCB in the bottom centre is a custom adapter board, which has an Analog Devices ADIS16475-2 IMU sensor soldered on to it. The PCB in the top left is the EtherCAT module, as provided by port GmbH. The connector on left side of the PCB couples the PCB to the wires leading to the external connectors mounted onto the lid of the enclosure.

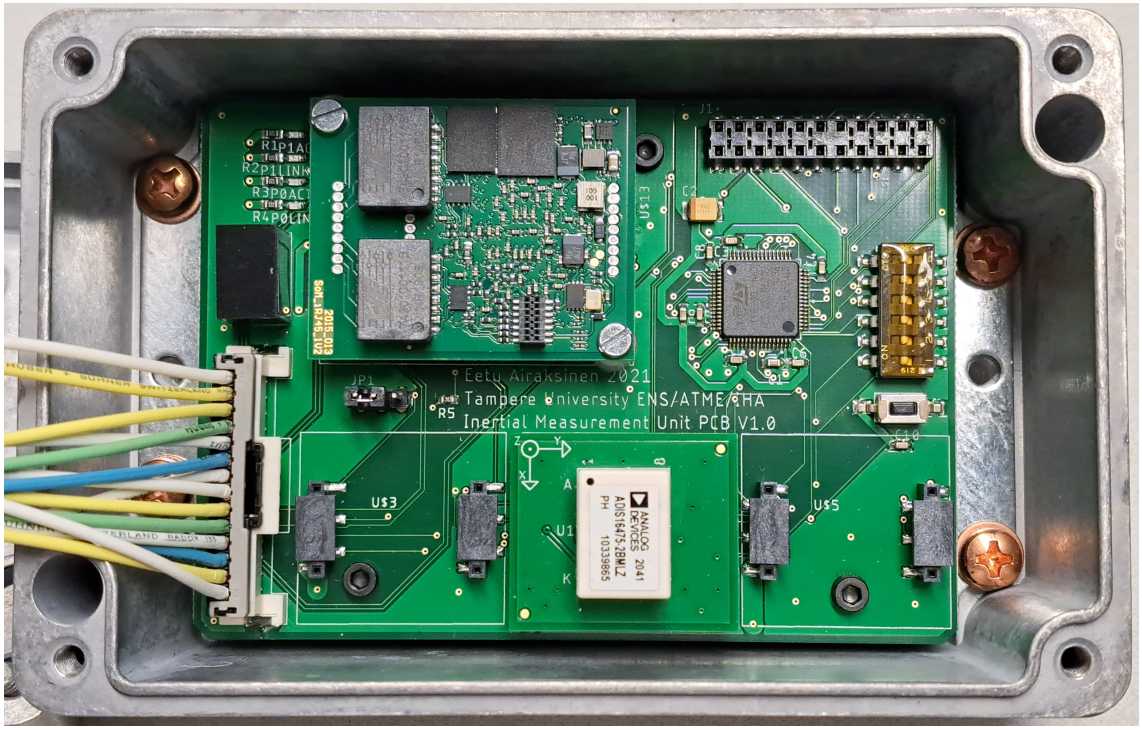

Figure 3.3. *Finished circuit boards as part of an assembled sensor node.*

3.4.2 Enclosure Assembly

The electronics were enclosed in diecast aluminium enclosures. The enclosures had rubber seals between the lid and the box, providing IP65 rating. The PCBs were fixed to inner steel panels using machine screws, nuts and nylon spacers. The lids of the enclosures were fitted with M8 connectors for EtherCAT and M12 connectors for power. The connectors had rubber O-rings between them and the enclosure lids, providing protection from the elements despite the holes they were mounted through.

A completed sensor enclosure can be seen in Figure 3.4. The orientation of the installed IMU was marked on the outside. This eliminated the need to open up the enclosure after installation on a MWM for figuring out the orientation of each individual sensor. In addition, each enclosure could be marked with an identification number.

The enclosures could be attached to the MWMs in different ways. For example, installing a metal plate to the bottom of an enclosure made it possible to attach the enclosure using straps. They could also be attached directly by screws to where holes could be drilled

into the machine for a more permanent installation.

Figure 3.4. *Completed sensor node enclosure.*

3.4.3 Firmware Flashing

The firmware was flashed onto the MCUs using an ST-LINK programming device, the license of which mentions that it should only be used in a research and development setting. The programmer was connected to the connector exposing the programming pins of the MCU and the board was powered through the onboard voltage regulator. Further details on flashing the firmware can be found in Appendix A.

3.5 Testing

The measurement node network was tested on a Hiab hydraulic boom, controlled by a Beckhoff automation controller. It was compared to the inertial measurement sensors the new network was supposed to replace. Both the accuracy and speed of the measurement network was tested.

For the test, the boom was operated with joysticks to produce motion, which would affect the readings of the inertial measurements of the sensor nodes. The measurement data was collected through the control automation system and saved onto a computer for later analysis. The data included the accelerometer data and the gyroscope data of each of

the three axes of five sensor nodes in the two sensor networks.

3.5.1 Integration into Heavy Machinery

The hydraulic Hiab boom, pictured in Figure 2.12 had the older IMU nodes shown in Figure **??** mounted onto it. The boom is controlled by a Beckhoff automation system, to which the older IMU nodes were connected using CAN bus. The new IMU nodes to be tested were mounted next to the old ones so that the data provided by them would be reasonably simple to compare. Figure 3.5 shows an installed sensor node in detail. Even though the new nodes were installed in relative orthogonality to the old nodes, some of the measurement axes of the new nodes did not match with the axes of the old nodes. This could be worked around, however. For example, a different axis, parallel to the axis of interest, could be chosen. If the axes point to opposite directions, a negation of one of them can be used instead. This way the data from adjacent sensors can be easily and relatively accurately compared.

The Hiab boom had absolute angle encoders and current loop sensors on an EtherCAT network. The new IMUs were connected to the same network, between these existing sensors. The Beckhoff system acted as the EtherCAT master for the network, with the sensors as slaves.

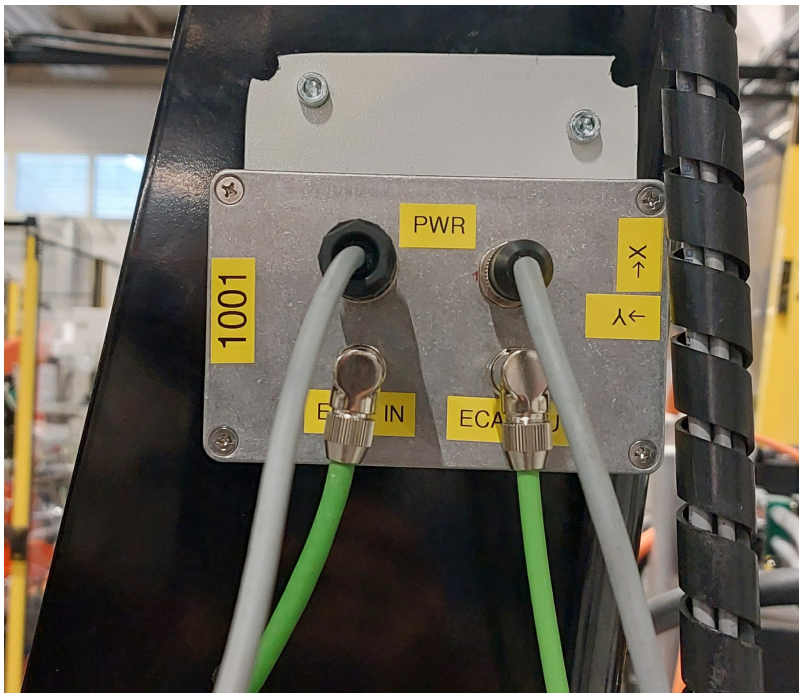

Figure 3.5. *A completed sensor node, installed onto the Hiab hydraulic boom.*

3.5.2 Test Results

The new sensor nodes were tested against the older IMU sensor system. With both measurement systems installed, the hydraulic boom was operated so that the inertial measurements of the movements could be recorded. Figures 3.6 and 3.7 show snippets of the recorded measurements. Any constant differences in the amplitude of the signals is attributable to slight scaling and misalignment errors. The quality of the data is still comparable.

In Figure 3.6, the accelerometer readings of the new IMUs are compared to the readings from the pre-existing system. There are three key differences between the two. First, there is a slight phase shift, indicating a delay in the measurements provided by the older system. Time delays in measurements should be avoided in high-speed control systems, as they can lead to oscillations and other inaccuracies. They also makes the RT aspects of the control system moot.

The second difference in the signals of Figure 3.6 relates to the smoothness of the signals. The signal from the new system appears to be much more noisy when compared to the one from the older system. The new system applies practically no filtering to its measurements, making the data instantaneous and more precise, while also allowing noise to pass through. The older system did not have any kind of filtering in place either. As the measurements can be filtered by the control system as needed, there is no advantage in withholding precise data by filtering it in the measurement node. The difference in noise is most likely attributable to differences in sensor resolution and especially communication speed.

The third difference that can be clearly seen in Figure 3.6 seems to be an intermittent error. The value from the older system appears to freeze from time to time. This could be caused by any number of problems, such as communication issues between the node and the automation controller, unintentional resetting of the node or faults in the IMU sensor itself, for example. The most likely reason is again the communication interface, as CAN is not a hard RT interface and can fail to communicate properly if overloaded with too much data, such as the measurement data of five 6 DOF IMUs. This kind of an error is not acceptable in mission critical motion control systems and can lead to very dangerous situations. The new system did not present such problems during testing.

In Figure 3.7, the gyroscope readings of the new IMU system are compared to the readings from the pre-existing system. With the angular velocity measurements there is only one major difference. A phase shift is present in these signals as well, which is to be expected, based on the acceleration measurement signals. The amount of noise in the two gyroscope signals appears to have no major differences. It should be noted that the intermittent errors plaguing the accelerometer signal of the older system seem to be ab-

sent from the gyroscope signal. This is peculiar but could still be attributable to an error in communications or other common factors.

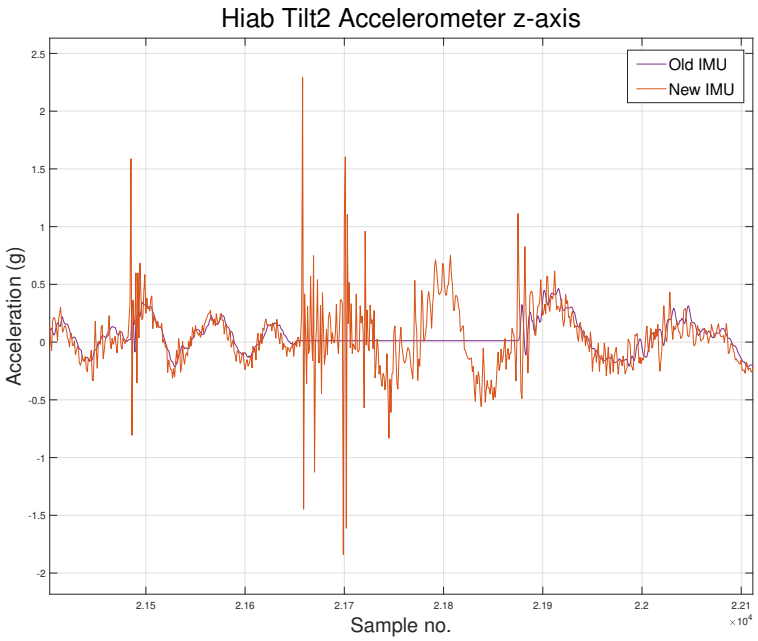

Figure 3.6. *Comparison of the accelerometer readings between the different IMUs.*

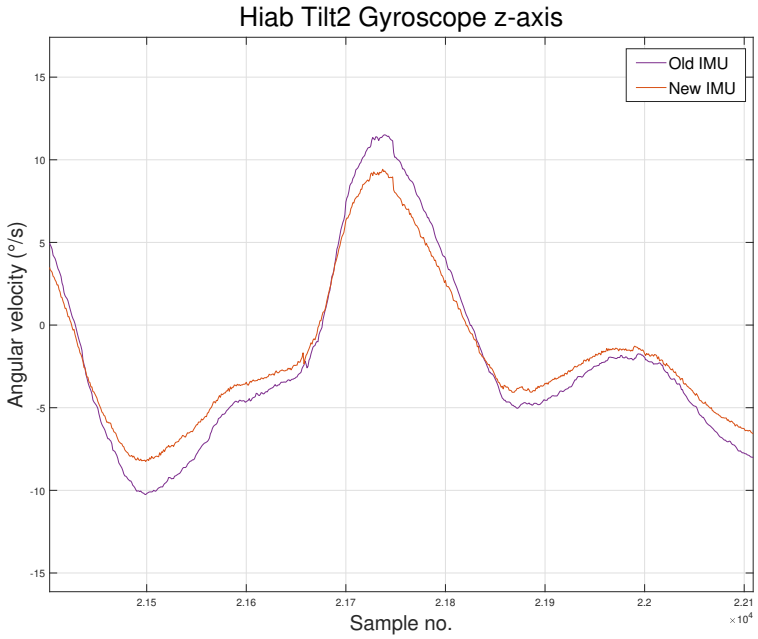

Figure 3.7. *Comparison of the gyroscope readings between the different IMUs.*

4. CONCLUSION

The aim of this thesis was to design, prototype and test an inertial measurement sensor network. The work was started by defining the requirements for the system, listed in Table 2.6. Based on the requirements, the overall functional concept was drawn up and component selections made. With the concept and component selections ready, the electrical design of the devices could be done. As the hardware got finalised, the firmware could be started to be worked on. When the work on the devices finished, they could be tested against the requirements and the older inertial measurement system previously used for research. The new system met the requirements set for it and clearly outperformed the system it was meant to replace.

Overall, this thesis reached its goals. There were several obstacles and hindrances, causing the work to be delayed and changing the scope of the thesis. The result, however, is a functional, flexible and expandable device. The performance of the nodes themselves is more than enough for the original use case and the data transfer capability of the network should not get saturated easily either. The network is well suited for research purposes and should enable future research into sensor fusion using many different types of sensors.

The journey of turning a concept into a finished device was exceptionally educating. Product development is a multistage process with many interwoven details to consider. Decisions made in very early stages can have surprising effects much later on. Optimally, the design should be iterated on to iron out any kinks. In this case, iteration was not possible, but some changes can be implemented in later stages of the lifetime of the design. After the initial prototype production run, some small additions were made to the design, based on user feedback and unforeseen needs. The revised design was used when getting additional units produced and further revisions may still be made should the need arise.

The modularity of the design lends itself well to further development. New sensors and other devices can be implemented using the interchangeable custom modules. A custom module with a wireless local area network chip has already been tested for use in wheel rotation sensor nodes similarly as in [32].

In addition to the expandability of the hardware, a lot of untapped potential lies in the software development aspects of the devices. For example, one feature that has been

requested is the ability to configure the IMUs remotely through EtherCAT. This should be possible with some changes to the firmware. The processing power of the nodes could also be harnessed in some use cases for pre-processing the data or even for implementing localised control systems.

REFERENCES

[1] *Stream - Smart Tools Railway work safEty and performAnce iMprovement*. URL: https://streams2r.eu/ (visited on 01/14/2022).

[2] Machado, T., Ahonen, A. and Ghabcheloo, R. *Towards a Standard Taxonomy for Levels of Automation in Heavy-Duty Mobile Machinery*. Accepted: 2022-01-25T22:03:15Z ISSN: 6037-3644. American Society of Mechanical Engineers, Dec. 13, 2021. ISBN: 978-0-7918-8523-9. DOI: 10.1115/FPMC2021-70251. URL: https://trepo.tuni.fi/handle/10024/137129 (visited on 05/04/2023).

[3] Nurmi, J. *On Increasing the Automation Level of Heavy-Duty Hydraulic Manipulators with Condition Monitoring of the Hydraulic System and Energy-Optimised Redundancy Resolution*. Accepted: 2019-05-29T10:50:56Z. Tampere University of Technology, 2017. ISBN: 978-952-15-3974-9. URL: https://trepo.tuni.fi/handle/10024/114984 (visited on 06/29/2022).

[4] *Hiab - We keep everyday life moving*. Hiab. URL: https://www.hiab.com/en/media/newsroom/hiab-crane-tip-control (visited on 05/04/2023).

[5] *IBC | John Deere GB&IE*. URL: https://www.deere.co.uk/en/forestry/ibc/ (visited on 05/04/2023).

[6] Manner, J., Mörk, A. and Englund, M. Comparing forwarder boom-control systems based on an automatically recorded follow-up dataset. *Silva Fennica* 53.2 (2019). ISSN: 22424075. DOI: 10.14214/sf.10161. URL: https://www.silvafennica.fi/article/10161 (visited on 06/29/2022).

[7] Koivumäki, J., Zhu, W.-H. and Mattila, J. Energy-efficient and high-precision control of hydraulic robots. *Control Engineering Practice* 85 (Apr. 1, 2019), pp. 176–193. ISSN: 0967-0661. DOI: 10.1016/j.conengprac.2018.12.013. URL: https://www.sciencedirect.com/science/article/pii/S0967066118307238 (visited on 06/29/2022).

[8] Tran, T.-D. Q. and Nguyen, V.-H. Heading Estimation for Autonomous Robot Using Dual-Antenna GPS. *International Journal of Mechanical Engineering and Robotics Research* (2020), pp. 1566–1572. ISSN: 22780149. DOI: 10.18178/ijmerr.9.12.1566-1572. URL: http://www.ijmerr.com/index.php?m=content&c=index&a=show&catid=185&id=1533 (visited on 05/08/2023).

[9] Mattila, J., Koivumäki, J., Caldwell, D. G. and Semini, C. A Survey on Control of Hydraulic Robotic Manipulators With Projection to Future Trends. *IEEE/ASME Transactions on Mechatronics* 22.2 (Apr. 2017). Conference Name: IEEE/ASME Trans-

actions on Mechatronics, pp. 669–680. ISSN: 1941-014X. DOI: 10.1109/TMECH.2017.2668604.

[10] Honkakorpi, J., Vihonen, J. and Mattila, J. Sensor Module for Hydraulic Boom State Feedback Control. *International Journal of Fluid Power* 13.3 (Nov. 2012). Publisher: River Publishers, Inc., pp. 15–23. ISSN: 14399776. DOI: 10.1080/14399776.2012.10781057. URL: http://libproxy.tuni.fi/login?url=https://search.ebscohost.com/login.aspx?direct=true&AuthType=cookie,ip,uid&db=asn&AN=83698915&site=ehost-live&scope=site (visited on 07/07/2022).

[11] Vihonen, J., Mattila, J. and Visa, A. Joint-Space Kinematic Model for Gravity-Referenced Joint Angle Estimation of Heavy-Duty Manipulators. *IEEE Transactions on Instrumentation and Measurement* 66.12 (Dec. 2017). Conference Name: IEEE Transactions on Instrumentation and Measurement, pp. 3280–3288. ISSN: 1557-9662. DOI: 10.1109/TIM.2017.2749918.

[12] Zhang, X., Peltola, E. and Mattila, J. Joint angle estimation for floating base robots utilizing MEMS IMUs. *8th IEEE International Conference on Cybernetics and Intelligent Systems (CIS), Robotics, Automation and Mechatronics (RAM)*. IEEE International Conference on Cybernetics and Intelligent Systems (CIS) and IEEE Conference on Robotics, Automation and Mechatronics (RAM). IEEE, 2017, pp. 282–287. DOI: 10.1109/ICCIS.2017.8274788. URL: https://researchportal.tuni.fi/en/publications/joint-angle-estimation-for-floating-base-robots-utilizing-mems-im (visited on 10/03/2022).

[13] *Murata SCC1300-D02 Datasheet*. URL: https://www.mouser.com/datasheet/2/281/scc1300-d02_datasheet_v2.1-1697.pdf (visited on 07/15/2022).

[14] *IP ratings | IEC*. URL: https://www.iec.ch/ip-ratings (visited on 10/24/2022).

[15] Minhang Bao. *Analysis and Design Principles of MEMS Devices*. Amsterdam: Elsevier Science, 2005. ISBN: 978-0-444-51616-9. URL: http://libproxy.tuni.fi/login?url=https://search.ebscohost.com/login.aspx?direct=true&AuthType=cookie,ip,uid&db=e000xww&AN=166279&site=ehost-live&scope=site (visited on 06/17/2022).

[16] *ADIS16475 Datasheet and Product Info | Analog Devices*. URL: https://www.analog.com/en/products/adis16475.html (visited on 11/22/2021).

[17] *ADIS16485.pdf*. URL: https://www.analog.com/media/en/technical-documentation/data-sheets/ADIS16485.pdf (visited on 04/27/2023).

[18] *SCHA63T-K03-Datasheet-Full.pdf*. URL: https://www.murata.com/-/media/webrenewal/products/sensor/gyro/SCHA600/pdf/SCHA63T-K03-Datasheet-Full (visited on 12/15/2022).

[19] Groves, P. D. *Principles of GNSS, Inertial, and Multisensor Integrated Navigation Systems*. Norwood, UNITED STATES: Artech House, 2013. ISBN: 978-1-60807-

006-0. URL: http://ebookcentral.proquest.com/lib/tampere/detail.action?docID=1531533 (visited on 02/03/2023).

[20] IEEE Standard for Specifying and Testing Single-Axis Interferometric Fiber Optic Gyros. *IEEE Std 952-2020 (Revision of IEEE Std 952-1997)* (Feb. 2021). Conference Name: IEEE Std 952-2020 (Revision of IEEE Std 952-1997), pp. 1–93. DOI: 10.1109/IEEESTD.2021.9353434.

[21] Knezic, M., Dokic, B. and Ivanovic, Z. Topology aspects in EtherCAT networks. *Proceedings of 14th International Power Electronics and Motion Control Conference EPE-PEMC 2010*. Proceedings of 14th International Power Electronics and Motion Control Conference EPE-PEMC 2010. Sept. 2010, T1–1–T1–6. DOI: 10.1109/EPEPEMC.2010.5606688.

[22] *OxTS AV200 Datasheet*. URL: https://www.oxts.com/wp-content/uploads/2021/09/OxTS-AV200-Datasheet_210910.pdf (visited on 05/24/2022).

[23] *3DMGQ7 GNSSINS Datasheet*. URL: https://www.microstrain.com/sites/default/files/3DMGQ7%20GNSSINS%20Datasheet%20%288400-0133%29%20Rev%20A.pdf (visited on 05/23/2022).

[24] *IPESSA Nano Product Sheet*. URL: https://kindhelm.com/wp-content/uploads/2021/09/IPESSA-Nano-Product-Sheet.pdf (visited on 05/23/2022).

[25] *Ekinox Series Leaflet*. URL: https://www.sbg-systems.com/wp-content/uploads/Ekinox_Series_Leaflet.pdf (visited on 05/23/2022).

[26] *Simulink - Simulation and Model-Based Design*. URL: https://se.mathworks.com/products/simulink.html (visited on 11/22/2021).

[27] *EAGLE | PCB Design And Electrical Schematic Software | Autodesk*. URL: https://www.autodesk.com/products/eagle/overview (visited on 11/22/2021).

[28] *Simulink Coder Support Package for STMicroelectronics Nucleo Boards*. URL: https://se.mathworks.com/matlabcentral/fileexchange/58942-simulink-coder-support-package-for-stmicroelectronics-nucleo-boards (visited on 11/22/2021).

[29] *STM32F411RE - High-performance access line, Arm Cortex-M4 core with DSP and FPU, 512 Kbytes of Flash memory, 100 MHz CPU, ART Accelerator - STMicroelectronics*. URL: https://www.st.com/en/microcontrollers-microprocessors/stm32f411re.html (visited on 11/22/2021).

[30] *port GmbH industrial real time communication - SoM IoT based on RENESAS RIN32M3*. URL: https://www.port-automation.com/en/products/som-module-embedded/som-iot-based-on-renesas-rin32m3.html (visited on 11/22/2021).

[31] ETG.2200 EtherCAT, EtherCAT P and Safety over EtherCAT Slave Implementation Guide. ().

[32] Zhang, X. *Towards IMU-based Full-body Motion Estimation of Rough Terrain Mobile Manipulators*. Accepted: 2022-11-14T09:53:34Z. Tampere University, 2022. ISBN:

978-952-03-2651-7. URL: https://trepo.tuni.fi/handle/10024/143486 (visited on 04/28/2023).

APPENDIX A: IMU NODE HARDWARE IN MORE DETAIL

This is meant as an instruction manual for an end user of the IMU node hardware. As such, it provides information on different interfaces available on the device and instructions for reprogramming the device if needed. The nominal specifications of the device are also included. The printed circuit board includes an STM32F411RE -microcontroller with an internal oscillator. Almost all of the pins of the microcontroller are accessible in one form or another on the board. Some of them are used for headers meant for communication or sensors. Some of them are connected to DIP switches for in-the-field configuration.

A.1 External Connectors

The device casing has four exposed connectors. Their pinouts are shown in Figure A.1. The connectors are:

- 2 M8 connectors for EtherCAT
- 2 M12 connectors for power

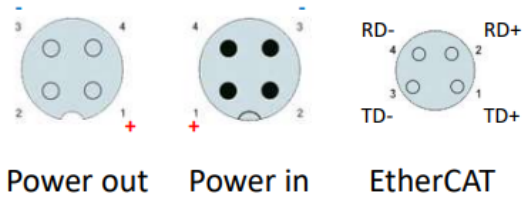

Figure A.1. *Connector pinouts.*

A.2 Internal Connectors

The internal board has the following connectors:

- 1 Connector for programming and reserved I/O
- 1 EtherCAT module connector
- 3 Connectors for sensor modules

- 1 External interface connector

All of the internal connectors and other components on the PCB are shown in Figure A.2. The pins available on the various connectors might have some alternate functions not listed in this document. For these functions, an interested reader should refer to the datasheet of the microcontroller.

The reserve connector has the programming interface of the STM32F411RE microcontroller exposed, as well as some other extraneous inputs and outputs. The programming interface can also be used for additional I/O if absolutely necessary. The pinout of the reserve connector is listed in Table A.1.

The EtherCAT module connector is specifically meant for accepting an iRJ45 SOM by port GmbH. It provides the module with power, an SPI bus for communicating with the microcontroller and connections to the external EtherCAT connectors. The communication bus is **SPI1** with **MISO = PA6**; **MOSI = PA7** and **SCLK = PA5**.

The connectors for sensor modules are capable of accepting custom-made boards with sensors mounted on them. They provide the sensor modules with power, communication buses to the microcontroller and some additional I/O. The exposed buses are **SPI5** (**MISO = PA12**; **MOSI = PA10**; **SCLK = PB0**) and **I^2C2** (**SDA = PB9**; **SCL = PB10**). The pinout of these connectors can be found in Table A.2.

The external interface connector connects to a plug, which is connected to the external connectors of the device. These connectors are the ones described in section A.1. The pinout of the connector is as shown in Table A.3.

A.3 Switches

There is a bank of 6 DIP switches on the board for in-the-field configuration. One side of the switches is connected to ground. The state of the switches can be read in software using pins listed in Table A.4. The switches do not have external pull-up resistors associated with them. This means that the software must configure the input pins to use the internal pull-up resistors of the microcontroller.

A.4 Programming

To flash program code to the node board, an ST-LINK programming device needs to be connected using the Serial Wire Debug (SWD) interface available on the reserve/programming connector. Refer to Table A.1 and the documentation of the particular programming device in use to properly connect the SWD pins. The board must be powered either through the onboard regulator or with a regulated power supply during programming. In addition, the Boot mode selector jumper needs to be set to the position closest to the external

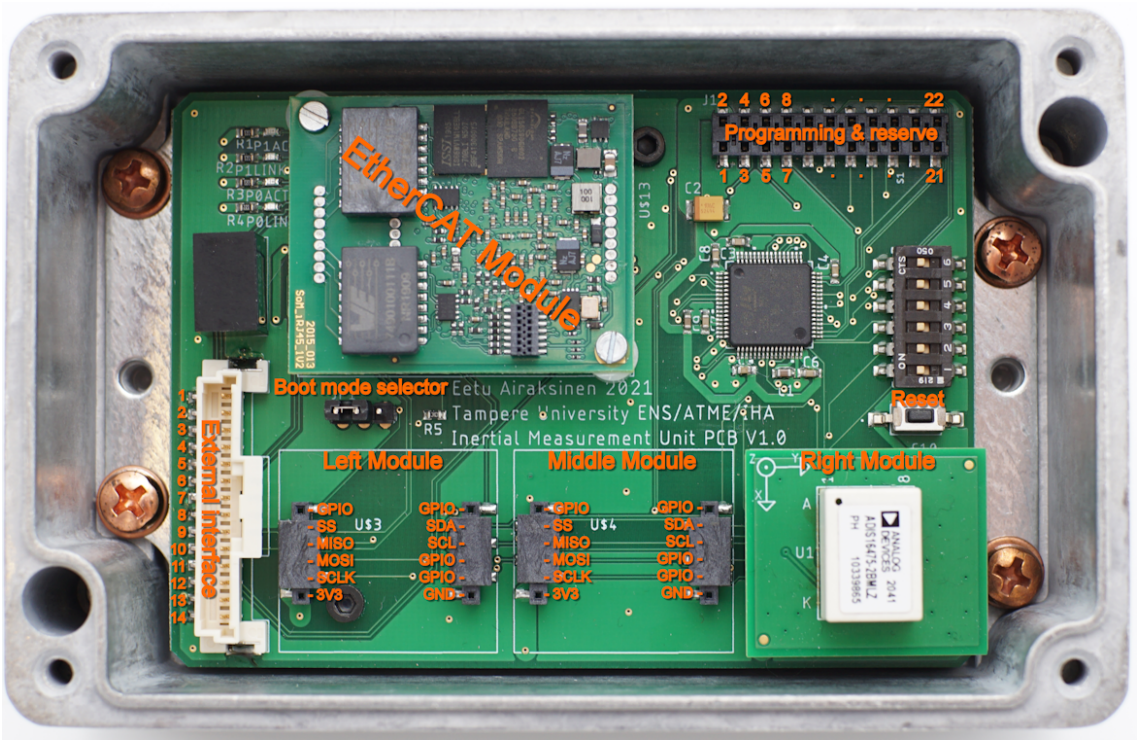

Figure A.2. *PCB with connectors.*

interface connector. The microcontroller can be programmed normally with properly compiled binaries. Using Simulink Coder Support Package for STMicroelectronics Nucleo Boards, Simulink should be able to utilize the ST-LINK to flash the desired code onto the microcontroller as well.

A.5 Specifications of node hardware

- Size (L x H x W): $121.2\,\text{mm} \times 41.3\,\text{mm} \times 65.5\,\text{mm}$
- Supply voltage: $4.75 \ldots 32$ VDC
- Microcontroller: STM32F411RE
  - Internal oscillator @ 100 MHz

Pin	Function	Pin	Function
1	GND	2	3V3
3	N/C	4	PC13
5	PC7	6	PC12
7	PC8	8	PC11
9	PC9	10	PC10
11	PB4 (JTRST)	12	PB3 (JTDO_SWO)
13	PA15 (JTDI)	14	PA14 (JTCK_SWCLK)
15	PA13 (JTMS_SWDIO)	16	PB5 (I^2C1_SMBA)
17	PB7 (I^2C1_SDA/USART1_RX)	18	PB6 (I^2C1_SCL/USART1_TX)
19	PA1 (SPI4_MOSI)	20	PA11 (SPI4_MISO)
21	PB13 (SPI4_SCK)	22	PB12 (SPI4_NSS)

Table A.1. *Pinout of programming and reserve connector.*

Left Module		Middle Module		Right Module	
Left conn.	Right conn.	Left conn.	Right conn.	Left conn.	Right conn.
PA8	PA9	PB1	PB2	PB14	PB15
SS (PA2)	SDA	SS (PA3)	SDA	SS (PA4)	SDA
MISO	SCL	MISO	SCL	MISO	SCL
MOSI	PH1	MOSI	PH0	MOSI	PC15
SCLK	PB8	SCLK	PD2	SCLK	PC14
3V3	GND	3V3	GND	3V3	GND

Table A.2. *Pinouts of sensor module connectors.*

Pin	Function
1	GND
2	12V
3	RX0_N
4	RX0_P
5	TX0_N
6	TX0_P
7	Shield
8	Shield
9	RX1_N
10	RX1_P
11	TX1_N
12	TX1_P
13	12V
14	GND

Table A.3. *Pinout of external interface connector.*

Switch	GPIO Pin
1	PC5
2	PC4
3	PC3
4	PC2
5	PC1
6	PC0

Table A.4. *GPIO pins the DIP switches are connected to.*